Multibody Syst Dyn (2016) 38:101–136
DOI 10.1007/s11044-016-9523-x

Analysis of collocated feedback controllers for four-bar planar mechanisms with joint clearances

Narendra Akhadkar[1] · **Vincent Acary**[2] · **Bernard Brogliato**[2]

Received: 22 June 2015 / Accepted: 10 May 2016 / Published online: 7 June 2016

Abstract This article presents an analysis of planar four-bar mechanisms with joint clearance when one joint is actuated by collocated open-loop or state feedback controllers (proportional-derivative, state feedback linearization, passivity-based control). The study is led with numerical simulations obtained with a projected Moreau–Jean's event–capturing algorithm. The contact/impact model uses kinematic coefficients of restitution and Coulomb's friction. The focus is put on how much the performance deteriorates when clearances are added in the joints. It is shown that collocated feedback controllers behave in a very robust way.

Keywords Four-bar mechanism · Clearance · Dynamic backlash · Unilateral constraints · Coulomb's friction · Impacts · Feedback control · Passivity-based control · State feedback linearization · Moreau–Jean time-stepping scheme

1 Introduction

A four-bar mechanism is the simplest form of closed chain linkage. It is widely used in many industrial applications. A closed chain linkage may be used, for transmission or transformation of motion, to precisely reach the desired position or orientation. Usually, the performance of a closed chain linkage is not as desired due to the manufacturing tolerances on links, clearance in the joints, and the assembly tolerances. However, the effects of clearance in the joints are different from link dimensional tolerances. The link dimensional tolerance leads to deviation in position and orientation, which are predictable and repeatable. A joint clearance is a hard highly nonlinear disturbance inducing an increase of degrees of freedom, and it may lead to uncertainty in the output position and motion, which may deteriorate the performance of industrial applications [87].

✉ B. Brogliato
bernard.brogliato@inria.fr

1 Schneider Electric, 31 avenue Pierre Mendès France, 38320 Eybens, France

2 INRIA Grenoble, Université Grenoble-Alpes, 655 avenue de l'Europe, Inovallée, 38334 Saint-Ismier, France

These deviations between design and real behavior motivated many researchers in mechanical engineering [18, 19, 22, 28, 32, 36, 37, 44, 48, 72, 73, 79] to study the revolute joints with imperfections. Proper modeling of the joint clearances in a multibody mechanical system is required to predict the behavior of real systems. Different contact models and simulation tools are available [35]. In the experimental and numerical study of planar slider crank and four-bar mechanism with multiple revolute clearance joints [24, 27, 32, 37], the influence of clearances on the performance of the system is demonstrated. The degradation of the system performance is always in the form of vibration, noise, very high reaction forces at the joints, precision, and accuracy of the output. The dynamic response of the system due to the joint clearances is more complex and tends to be chaotic in some situations [26, 28, 64, 71, 72, 75, 88]. To reduce or alleviate this chaotic behavior, delayed feedback control [64], optimization of various physical parameters [23–25, 88], or redundant actuators that guarantee suitable preload for backlash avoidance in parallel manipulators [60] have been proposed.

In parallel with multibody modeling and numerical simulation, feedback controllers have been proposed with the purpose of increasing the motion accuracy of systems with clearances. This is called *backlash compensation* in the systems and control literature [45, 62]. Two major classes of models are used: dead-zone and hysteresis models, also called static backlash [15, 81, 82, 90], which are suitable for feedback control design but completely neglect the contact/impact dynamics, and dynamic backlash with compliant spring/dashpot models [46, 61]. Few studies use dynamic backlash with nonsmooth, set-valued models [40, 52]. Static and dynamic models of backlash yield quite different harmonic properties [17].

Most, if not all, of the multibody-oriented above studies and some of the control-oriented ones use the contact/impact phenomena in the clearances with compliant, linear, or nonlinear spring/dashpot models (this is even sometimes stated as a basic modeling requirement [65]) and regularized Coulomb's friction [49, 88]. It is worth noting that we are dealing here with contact that may be conformal, especially if clearances are small compared to bearing and journal diameters. In such a case, the Hertz elasticity may not be suitable, to say nothing about linear elasticity. An additional modeling issue concerns energy dissipation via viscous friction and which damping model should be chosen: linear or nonlinear (like the Hunt–Crossley or Kuwabara–Kono models [9, Chap. 2])? Other models using some kind of bistiffness elasticity (like Walton–Braun, Lankarani–Nikravesh, and all their variants [9, §4.2])? This remains quite unclear to us. Moreover, it is quite often a hard task to estimate their parameters (equivalent stiffness and damping). A major drawback of such an approach is that the numerical stabilization of contact forces and accelerations during the persistent contact phases is not an easy task. Spurious oscillations may appear in the simulation of these contact modes (see e.g. [30, 35, 43, 63, 80, 88], [29, Figs. 4.22, 4.23]). Moreover, the regularization of Coulomb's law at zero tangential velocity (i.e., in the two-dimensional case, replacing the vertical segment of Coulomb's law characteristic by some finite-slope or sigmoid curve) has to be absolutely avoided since it cannot model properly the sticking modes, which play a significant role in the contact dynamics. In addition, contrarily to what is sometimes stated [67], very efficient numerical methods exist for the simulation of set-valued characteristics that we use in this work. Finally, the contact parameter estimation may be a hard task (especially, if both normal and tangential models depend on several parameters and impacts are considered), and stiff differential equations may appear due to very large contact equivalent stiffnesses. Therefore, nonsmooth, set-valued models that use few parameters but retain the major contact dynamics features may be preferred in many multibody multicontact applications.

Thümmel et al. [79] discussed the methodology for modeling mechanisms with clearance, friction, and impact within the so-called *nonsmooth contact dynamic method* (NSCD)

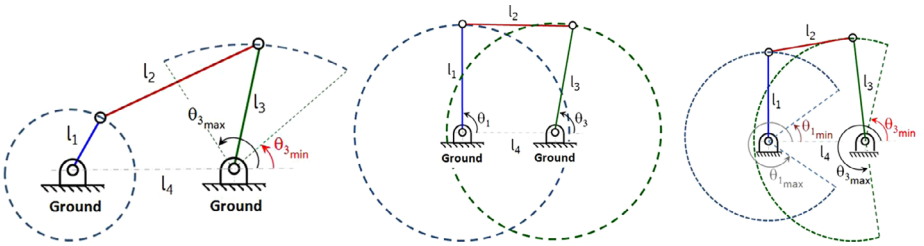

(a) Crank-rocker. (b) Crank-crank. (c) Rocker-rocker.

Fig. 1 Three types of four-bar mechanisms

introduced by Moreau and Jean [38, 39, 56, 58, 59]: the interaction between bodies is modeled with unilateral constraints, complementarity conditions, kinematic or kinetic restitution coefficients, and set-valued frictional models (like Coulomb's law) [9, 34, 69]. Following Moreau [57], the dynamics of rigid multibody systems is formulated at the velocity-impulse level. The NSCD has proved to be a quite efficient numerical method, capable of handling complementarity conditions, impacts, and set-valued friction laws [4, 78]. Further studies using the nonsmooth contact dynamics methods may be found in [31, 44, 79]. Careful comparisons between numerical and experimental data are reported in [44, 79, 83–86]: they show that the so-called time-stepping numerical schemes associated with set-valued force laws possess very good forecast capabilities. This motivates us to use the NSCD method, with the enhanced scheme derived in [2] and available in the INRIA open-source library SICONOS [4]. It is worth noting that all of the above analysis (as well as the one in this paper) deal with two-dimensional joints. Recently, the three-dimensional case has been tackled in [49, 89]. In such a case, cylindrical contact/impact models may be considered [68].

In this article, we study three different examples of the four-bar mechanism (crank–rocker, crank–crank, and rocker–rocker, see Fig. 1) controlled with six different inputs, mainly through numerical simulations. From a general point of view, joint clearances introduce nonsmooth, nonlinear perturbations and an increase of the system degrees of freedom, which render the controlled system *underactuated*.[1] Studying the robustness of (otherwise globally exponentially stable when applied on the ideal, no clearance system) controllers with respect to such hard disturbances is a tough task for at least two main reasons: (a) analyzing the effects of impacts on the closed-loop system's Lyapunov function derivative, is in general uneasy, especially in a trajectory tracking framework, where complete solutions have been proposed for fully actuated systems only [8, 11, 12, 33, 51, 54, 55]; (b) moreover, the system dynamics is strongly changed also between impacts due to the increase of the configuration space dimension, and the analysis of the ideal system Lyapunov function variation during the persistently constrained or unconstrained phases is also a hard task, which, to the best of the authors' knowledge, has never been tackled. Let us stress that our objective is not to derive new control strategies for backlash compensation, but to study both qualitatively and quantitatively how the addition of clearances modifies the controlled system behavior when well-known state feedback schemes are applied. Surprisingly enough, collocated feedback inputs possess remarkable robustness and drastically improve the system performance compared with open-loop control torques.

The article is organized follows. The dynamics are introduced in Sect. 2: the local kinematics that allows us to derive the gap functions in Sect. 2.1, the normal and tangential

[1] There are less actuators than degrees of freedom.

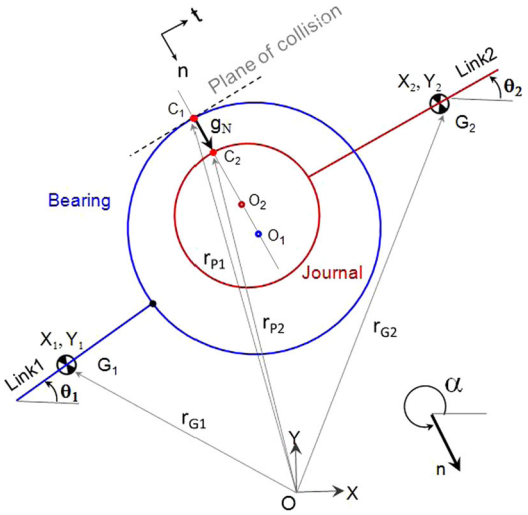

Fig. 2 Planar revolute joint with clearance in a multibody system

contact laws in Sect. 2.2, the Lagrange dynamics in Sect. 2.3, and a numerical scheme in Sect. 2.4. Section 3 is dedicated to the analysis of the four-bar systems with time-dependent open-loop control inputs. Four different feedback controllers are studied in Sect. 4: two proportional-derivative (PD) inputs in Sect. 4.1, a state feedback linearization in Sect. 4.2, and a passivity-based controller in Sect. 4.3. Conclusions end the article in Sect. 5. Details on the system dynamics and the closed-loop system stability analysis are given in the Appendix.

2 The Lagrange dynamics with unilateral constraints and Coulomb's friction

2.1 Modeling of revolute joints with 2D clearance

The local kinematics that allow us to derive the unilateral constraints are treated in detail in [4, 34, 69]. Let us provide its formulation for a generic revolute joint with radial clearance c as depicted in Fig. 2. In an ideal revolute joint, it is assumed that the centers of two interconnected bodies (journal and bearing) coincide. A revolute joint with clearance separates these two center points. It does not constrain any degree of freedom in the mechanical system like the ideal revolute joint. However, it imposes kinematic restrictions on the journal motion. Thus, an imperfect revolute joint introduces two degrees of freedom in the mechanical system. The radial clearance is defined as $c = r_1 - r_2$, where r_1 is the radius of bearing, and r_2 is the radius of journal ($r_1 > r_2$). In Fig. 2, O_1 and O_2 indicate the bearing and journal centers, and C_1 and C_2 represent the potential contact points on the bearing and journal, respectively. The $(O, \mathbf{i}, \mathbf{j})$ coordinate frame represents the inertial coordinate system (with coordinates X and Y). The vectors r_{C_1} and $r_{C_2} \in \mathbb{R}^2$ denote the positions of contact points C_1 and C_2 in the inertial coordinate system. The centers of mass of bodies 1 and 2 are G_1 and G_2 with coordinates (X_1, Y_1) and (X_2, Y_2), respectively. The bodies orientations are the angles θ_1 and θ_2. The vectors r_{G_1} and $r_{G_2} \in \mathbb{R}^2$ denote the positions of the bearing and journal centers of mass, whereas r_{O_1} and $r_{O_2} \in \mathbb{R}^2$ denote the positions of the centers of bearing and journal, both in the inertial coordinate system. The normal and tangential vectors to the

plane of collision between the bearing and the journal are defined by $(\mathbf{n}, \mathbf{t}) \in \mathbb{R}^2$. Note that the unit vector $\mathbf{n}$ has the same direction as the line of the centers of the journal and bearing. The orientation of $\mathbf{n}$ is chosen such that it always acts inward from the journal center to the bearing center. The signed distance (or gap function) is calculated as

$$g_N = (C_1C_2)^T\mathbf{n} = c - (O_2O_1)^T\mathbf{n}. \tag{1}$$

The magnitude of eccentricity (clearance) vector O_2O_1 is denoted by $\|O_2O_1\|$, and its orientation is given by α. The unit normal vector $\mathbf{n}$ is given as $\mathbf{n} = \frac{O_2O_1}{\|O_2O_1\|}$ with

$$\begin{aligned} O_2O_1 = &\left(X_1 + \frac{l_1}{2}\cos\theta_1 - X_2 + \frac{l_2}{2}\cos\theta_2\right)\mathbf{i} \\ &+ \left(Y_1 + \frac{l_1}{2}\sin\theta_1 - Y_2 + \frac{l_2}{2}\sin\theta_2\right)\mathbf{j}, \end{aligned} \tag{2}$$

$$\mathbf{n} = \cos\alpha\mathbf{i} + \sin\alpha\mathbf{j}, \qquad \mathbf{t} = -\sin\alpha\mathbf{i} + \cos\alpha\mathbf{j}, \tag{3}$$

$$\begin{aligned} \cos\alpha &= \left(\frac{X_1 + \frac{l_1}{2}\cos\theta_1 - X_2 + \frac{l_2}{2}\cos\theta_2}{\|O_2O_1\|}\right), \\ \sin\alpha &= \left(\frac{Y_1 + \frac{l_1}{2}\sin\theta_1 - Y_2 + \frac{l_2}{2}\sin\theta_2}{\|O_2O_1\|}\right). \end{aligned} \tag{4}$$

If we denote the generalized coordinates of each body as $q_i = (X_i, Y_i, \theta_i)^T$, $i = 1, 2$, then we obtain that $g_N = g_N(q_1, q_2)$. We also have $r_{C_1} = r_{G_1} + G_1C_1 = r_{G_1} + G_1O_1 + O_1C_1$ and $r_{C_2} = r_{G_2} + G_2C_2 = r_{G_2} + G_2O_2 + O_2C_2$. Differentiating these expressions with respect to time yields

$$\begin{cases} V_{C_1} = \frac{d}{dt}r_{G_1} + \frac{d}{dt}(G_1C_1) = \frac{d}{dt}r_{G_1} + \frac{d}{dt}(G_1O_1) + \frac{d}{dt}(O_1C_1), \\ V_{C_2} = e\frac{d}{dt}r_{G_2} + \frac{d}{dt}(G_2C_2) = \frac{d}{dt}r_{G_2} + \frac{d}{dt}(G_2O_2) + \frac{d}{dt}(O_2C_2), \end{cases} \tag{5}$$

which leads to

$$\begin{cases} V_{C_1} = \begin{pmatrix} \dot{X}_1 - (\frac{l_1}{2}\sin(\theta_1) - r_1\sin(\alpha))\dot{\theta}_1 \\ \dot{Y}_1 + (\frac{l_1}{2}\cos(\theta_1) - r_1\cos(\alpha))\dot{\theta}_1 \end{pmatrix}, \\ V_{C_2} = \begin{pmatrix} \dot{X}_2 - (\frac{l_2}{2}\sin(\theta_2) - r_2\sin(\alpha))\dot{\theta}_2 \\ \dot{Y}_2 + (\frac{l_2}{2}\cos(\theta_2) - r_2\cos(\alpha))\dot{\theta}_2 \end{pmatrix}, \end{cases} \tag{6}$$

where $V_{C_i} \in \mathbb{R}^2$ $(i = 1, 2)$ are the absolute velocities of the contact points. Consequently, the relative velocity of contact points is expressed in the local frame as

$$U = \begin{pmatrix} U_N \\ U_T \end{pmatrix} = \begin{pmatrix} (V_{C_2} - V_{C_1})^T\mathbf{n} \\ (V_{C_2} - V_{C_1})^T\mathbf{t} \end{pmatrix}. \tag{7}$$

From (6) and (7) the normal and tangential components of the relative velocity can be calculated:

$$\begin{pmatrix} U_N \\ U_T \end{pmatrix} = \begin{pmatrix} \cos\alpha & \sin\alpha & \frac{l_1}{2}\sin A & -\cos\alpha & -\sin\alpha & \frac{l_2}{2}\sin B \\ -\sin\alpha & \cos\alpha & -\frac{l_1}{2}\cos A + r_1 & \sin\alpha & -\cos\alpha & -\frac{l_2}{2}\cos B - r_2 \end{pmatrix} \begin{pmatrix} \dot{q}_1 \\ \dot{q}_2 \end{pmatrix}, \tag{8}$$

where $A = (\theta_1 - \alpha)$, $B = (\theta_2 - \alpha)$.

2.2 Normal and tangential contact laws

The contact force is denoted $R = (R_N, R_T)^T \in \mathbb{R}^2$ in the local frame $(\mathbf{n}, \mathbf{t})$. Due to the impenetrability assumption, we have $g_N(q) \geq 0$. We also neglect adhesive effects, so that $R_N \geq 0$. If $R_N > 0$, then we impose $g_N(q) = 0$, and when $g_N(q) > 0$, the normal contact force must vanish, that is, $R_N = 0$ (no magnetic or distance forces) [1, 4, 9]. These conditions yield a complementarity condition denoted compactly as

$$0 \leq g_N(q) \perp R_N \geq 0. \tag{9}$$

The normal contact law at the velocity level is expressed as

$$0 \leq U_N^+ + e_r U_N^- \perp R_N \geq 0 \quad \text{if } g_N(q) = 0, \tag{10}$$

where $U_N^+ = \nabla g_N(q)^T \dot{q}^+$ is the relative velocity after the collision, $U_N^- = \nabla g_N(q)^T \dot{q}^-$ is the relative velocity before the collision, and $e_r \in [0, 1]$ is the restitution coefficient.[2] The tangential contact law is based on Coulomb's friction law and is defined locally at each contact point ($C_1 = C_2$). In the 2D case Coulomb's friction law is as follows:

$$-R_T \in \mu |R_N| \operatorname{sgn}(U_T), \tag{11}$$

where $\mu \geq 0$ is the coefficient of friction, and $\operatorname{sgn}(\cdot)$ is the set-valued signum function with $\operatorname{sgn}(0) = [-1, 1]$. It is worth noting that the basic Coulomb law can be easily enhanced with static and dynamic friction coefficients, varying friction coefficient (with Stribeck effects), or micro-displacements during sticking modes, while staying in a set-valued context that is suitable for a proper time-discretization including sticking modes [4, §3.9].

2.3 Lagrangian formulation with bilateral and unilateral constraints

Let us consider a Lagrangian mechanical system with generalized coordinate vector $q \in \mathbb{R}^n$ and subjected to m constraints, with m_b holonomic bilateral constraints $g_N^\alpha = 0$ and $\alpha \in \mathcal{E}$, m_u unilateral constraints $g_N^\alpha \geq 0, \alpha \in \mathcal{I}$, and $m = m_b + m_u = |\mathcal{E}| + |\mathcal{I}|$, and with 2D Coulomb friction. The Lagrangian formalism of such a system is as follows [4, 69]:

$$\begin{cases} \dot{q}(t) = v(t), \\ M(q(t))\dot{v}(t) + F(t, q(t), v(t)) = G_N^\top(q(t))R_N + G_T^\top(q(t))R_T, \\ g_N^\alpha(q(t)) = 0, \quad \alpha \in \mathcal{E}, \\ \left.\begin{array}{l} g_N^\alpha(q(t)) \geq 0, \qquad R_N^\alpha \geq 0, \qquad R_N^\alpha g_N^\alpha(q(t)) = 0, \\ U_N^\alpha(t^+) = -e_r^\alpha U_N^\alpha(t^-) \quad \text{if } g_N^\alpha(q(t)) = 0 \quad \text{and} \quad U_N^\alpha(t^-) \leq 0, \\ -R_T^\alpha \in \mu^\alpha R_N^\alpha \operatorname{sgn}\big(U_T^\alpha\big) \quad \text{if } g_N^\alpha\big(q(t)\big) = 0, \end{array}\right\} \quad \alpha \in \mathcal{I} \end{cases} \tag{12}$$

where $v(t)$ is the vector of generalized velocities, $M(q) \in \mathbb{R}^{n \times n}$ is the mass matrix, $F(t, q, v) = C(q, v)v - \mathbf{g}(q) - B\tau(t, q, v) \in \mathbb{R}^n$ is the vector of generalized forces, $C(q, v)v \in \mathbb{R}^n$ is the vector of Coriolis and gyroscopic forces, $\mathbf{g}(q)$ contains forces derived

[2] When friction is present during impacts, there is in general no reason that e_r should be upper bounded by 1; see [9, Chap. 4]. Moreover, inertial couplings may introduce kinetic energy increase for nearly elastic impacts. Finally, dynamical singularities like Painlevé paradoxes may occur during sliding motions [9, Chap. 5]. We have not noticed such issues in the particular cases treated further with small friction coefficients.

from a potential, $B \in \mathbb{R}^n$ is the input matrix, $\tau(t, q, v)$ is the scalar control torque applied at joint J_1 (see Fig. 3 below), and $G_N(q) = \nabla g_N(q)^T \in \mathbb{R}^{m\times n}$ and $G_T(q) \in \mathbb{R}^{m\times n}$ are the linear maps of local normal and tangent frames at the contact points (i.e., $U_T = G_T(q)\dot{q}$ and $U_N = G_N(q)\dot{q}$; see (8)).

In the sequel, we consider only unilateral constraints since bilateral constraints are eliminated by coordinate reduction. Details on the dynamics of the four-bar systems are provided in Appendices A, A.1, and B.

Remark 1 (i) The mathematical well-posedness of the Lagrange dynamics in (12) has been shown in the frictionless case in [6, 20, 21, 66]; in the case with friction, see [7, 76]. (ii) When there is no clearance, $n = 1$, and the system is fully actuated. When one clearance is present (resp. two clearences), $n = 3$ (resp. $n = 5$), and the system becomes underactuated. (iii) Various contact/impact models are compared in [29]. It is not obvious to determine which model is the best. The approach chosen in this article seems to be a suitable compromise for many physical effects occurring in joints with clearance and which are quite difficult to encapsulate in a single contact/impact model with a reliable numerical method (dissipation at impacts, friction, conforming/non conforming contacts). As alluded to above, it may be enhanced while staying in the same overall rigid body framework.

2.4 The numerical integration method

The numerical time-integration scheme used in this article is an event–capturing time-stepping method mainly based on the Moreau–Jean time-stepping scheme [38, 39, 56, 58, 59]; see also [70, 77] for a similar time-stepping scheme. As we said in the Introduction, the method uses a formulation of the dynamics at the velocity/impulse level that enables a very robust numerical time-integration of systems with a lot of impact events. Contrary to event-driven schemes, the events are not accurately located in time but integrated within the time-step. Although this leads to robust schemes, the treatment of the constraints and the impact law at the velocity level yields drift at the position level. When we study multibody systems with clearances in joints with unilateral contact, we need to keep the drift of the constraints as small as possible with respect to the characteristic lengths of the clearances.

This is the reason why we use a scheme that satisfies constraints both at the velocity and position levels. It is an extension of the Moreau–Jean scheme together with the Gear–Gupta–Leimkuhler (GGL) method to systems with unilateral constraints and impacts [2]. Applying directly the GGL approach to unilateral constraint may yield to spurious oscillations at contact that depend on the activation procedure of the constraints at the velocity level. In [2], this issue is fixed by consistently activating the constraints within the time-step in an iterative way. Especially, we want to avoid the projection onto a constraint if the associated constraint at the velocity level is not activated. The so-called "combined scheme" is based on the iterations denoted by ν of the following two steps:

1. The *projection step* is based on the solution of the following system:

$$\begin{cases} M(q_{k+\theta})(v_{k+1}-v_k) - hF_{k+\theta} = G(q_{k+1})P_{k+1}, \\ q_{k+1} = q_k + hv_{k+\theta} + G(q_{k+1})\gamma_{k+1}, \\ U_{k+1} = G^\top(q_{k+1})v_{k+1}, \\ g_{k+1} = g(q_{k+1}), \\ \text{for all } \alpha \in \mathcal{I}^\nu, \begin{cases} 0 \le U^\alpha_{N,k+1} + eU^\alpha_{N,k} \perp P^\alpha_{N,k+1} \ge 0, \\ -P_{T,k+1} \in \mu^\alpha P^\alpha_{N,k+1}\ \mathrm{sgn}(U^\alpha_{T,k+1}), \\ g^\alpha_{k+1} = 0, \gamma^\alpha_{k+1} \quad \text{if } P^\alpha_{N,k+1} > 0, \\ 0 \le g^\alpha_{k+1} \perp \gamma^\alpha_{k+1} \ge 0 \quad \text{otherwise}, \end{cases} \end{cases} \tag{13}$$

   for a given index set $\mathcal{I}^\nu$ of active constraints. The time-step is denoted by h, and the notation $x_{k+\theta} = (1-\theta)x_k + \theta x_{k+1}$ is used for $\theta \in [0,1]$. Compared to the Moreau–Jean scheme, the multiplier γ_{k+1} is added to improve the constraint drift. Note that P_{k+1} is an impulse that remains always bounded when an impact occurs.
2. The *activation step* computes the index set $\mathcal{I}^\nu$ of active constraints by checking for a given value of g_{k+1} if the constraint is satisfied or not. Starting form $\mathcal{I}^0 = \emptyset$, at each iteration ν, the activation performs the following operation:

$$\mathcal{I}^{\nu+1} = \mathcal{I}^\nu \cup \left\{\alpha \in \mathcal{I} \mid g^\alpha_{k+1} \le 0\right\}. \tag{14}$$

The iterates (q_{k+1}, v_{k+1}) of the solution depend on the iteration number ν. In order to avoid useless complexity in the notation, we skip the superscript ν when there is no ambiguity. Steps 1 and 2 are iterated until the index set $\mathcal{I}^\nu$ is constant. The algorithm can be extended straightforwardly to the frictional case.

The contact events are not detected with high precision in such event–capturing methods, and the number of calculated impacts depends on h. In the next section, the choice $h = 10^{-5}$ s is made. Computations reported in [4, Table 14.2] show that this is a reasonable time step, and smaller h is not necessary, because the collisions that are not detected have negligible influence on the system dynamics (in particular, on the kinetic energy loss). The simulations in this article have been led with the code implemented in the INRIA open-source software SICONOS.[3]

Remark 2 Two major classes of numerical methods exist: event-driven and event–capturing (or time-stepping) schemes. They both possess advantages and drawbacks. In case of systems that undergo a large number of events (like stick/slip transitions and impacts), event–capturing methods are preferable despite their low order [4, 78] because event-driven strategies rapidly become cumbersome to implement and too time-consuming. Moreover, event–capturing methods have been proved to converge and to possess nice energetic properties [3].

2.5 Analysis methodology

Let us consider a four-bar mechanism (see Fig. 3(a,b)) with bodies of mass m_i, length l_i, and inertia I_i, $1 \le i \le 3$. An imperfect joint is defined by a unilateral constraint $g_j = (c_j - O_jO_{j-1}\mathbf{n}) \ge 0$, $j = 2$ or 3, where c_j is the radial clearance at the imperfect joint. The four-bar mechanism with clearance in one revolute joint is described by three generalized

[3] http://siconos.gforge.inria.fr/.

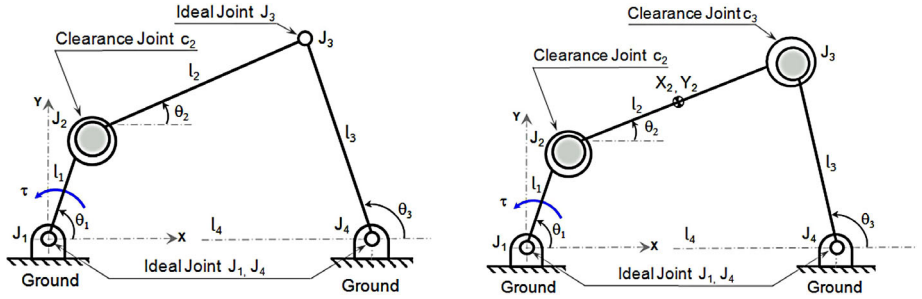

(a) Clearance in joint J_2. (b) Clearance in joint J_2 and J_3.

Fig. 3 Four-bar mechanism with clearance in revolute joints

coordinates $q = [\theta_1, \theta_2, \theta_3]^T$ and that with clearance in two revolute joints it is described by five generalized coordinates $q = [\theta_1, \theta_2, \theta_3, X_2, Y_2]^T$. The four-bar mechanism is actuated at the joint 1 (J_1). We consider joints J_1 and J_4 to be perfect revolute joints, whereas the joints J_2 and J_3 may be imperfect with radial clearances c_2 and c_3. The influence of different clearance sizes c_2 and c_3, coefficient of restitution (e_r), and coefficient of friction (μ) on the mechanism performance is studied. Results are compared with the cases without clearance and without friction. The presence of clearance in the revolute joint can lead to variation in the initial conditions, and this variation depends on the value of the radial clearance. To this aim, in the first step, we study the influence of the initial conditions on the system long-term behavior with perfect revolute joints. Let $\|\cdot\|_\infty$ be defined as[4] $\|X\|_\infty = \max_{t\in[1,10]} |X(t)|$. The percentage relative error in the angular position $\theta_1(0)$ is given as

$$e_0 = \frac{\|\theta_1^{i1}(t) - \theta_1^{idl}(t)\|_\infty}{\|\theta_1^{idl}(t)\|_\infty} \times 100, \tag{15}$$

where $\theta_1^{idl}(t)$ is the angular position of links with the reference initial condition, and $\theta_1^{i1}(t)$ is the angular position of links with different initial conditions. We plot the isolines of the percentage relative error e_0 with $\theta_1(0)$ and $\dot{\theta}_1(0)$. In the second step, we analyze through numerical simulations how much the presence of clearances deteriorates the system dynamical behavior. The percentage relative error in the angular positions θ_1 and θ_3 is given as

$$e = \max_{p\in\{1,3\}} \frac{\|\theta_p^{cl}(t) - \theta_p^{id}(t)\|_\infty}{\|\theta_p^{id}(t)\|_\infty} \times 100, \tag{16}$$

where $\theta_p^{id}(t)$ is the angular position of links without joint clearance, and $\theta_p^{cl}(t)$ is the angular position of links with joint clearance. The contour plot with different levels of isolines represents the variation of error in the angular position. In the second step, the initial conditions remain constant, and only radial clearances (c_2 and c_3) are varied for different values of coefficients of restitution e_r and of friction μ. For all contour plots, simulations are carried out for every 0.5 mm increment in joint clearance and for every 0.1 increment in coefficient of restitution. Therefore, the error e allows us to analyze the loss of performance of a controller when clearances are added and is different from the usual tracking error that is widely

[4]The first initial period [0, 1] s is not included in the infinity norm in order to eliminate the transient period, and we concentrate ourselves on the steady-state behavior of trajectories only.

used in the control literature. It measures the proximity between the cases with and without mechanical play.

3 Open-loop control

In this section, two open-loop[5] inputs τ are considered: a constant torque $\tau_1 = 6.0\,\mathrm{N\,m}$ and a sinusoidal torque $\tau_2 = 6.0\sin(0.75\pi t)\,\mathrm{N\,m}$, applied at the joint J_1 in counter-clockwise direction. Since our main goal is comparison of feedback controllers and since the results we obtained for the three types of four-bar mechanisms were quite similar, only the crank–rocker case is presented. Let us consider a crank–rocker mechanism as in Fig. 1(a), where the input link l_1 rotates fully (360°), and the output link l_3 oscillates through angles $\theta_{3_{\min}}$ and $\theta_{3_{\max}}$. Geometric and inertial properties of the crank–rocker four-bar mechanism are given in Table 1. The initial conditions are $\theta_1(0) = 1.571$ rad, $\theta_2(0) = 0.3533$ rad, $\theta_3(0) = 1.2649$ rad, and $\dot{\theta}_1(0) = \dot{\theta}_2(0) = \dot{\theta}_3(0) = 0.0$ rad/s. The coordinates of the center of gravity of link 2 are $X_2 = 1.8764$ m, $Y_2 = 1.6919$ m. The parameters used for the dynamic simulation are given in Table 2. The deviation in the system performance is studied with the percentage relative error in angular position e_0 in (15) to find out the sensitivity to the initial conditions. The results are depicted in Fig. 4. The major conclusion is that the system sensitivity w.r.t. initial conditions changes drastically when the constant torque is replaced by a sinusoidal one: Fig. 4(a) shows an ordered behavior with horizontal stripes (zero gradient of $e_0(\theta_1(0))$) and small gradient of $e_0(\dot{\theta}_1(0))$, whereas Fig. 4(b) shows a disordered behavior with a high gradient of $e_0(\theta_1(q), \dot{\theta}_1(0))$ between the isolines, indicating high sensitivity.

Let us now analyze the case with one clearance in joint J_2. The numerical simulations are depicted in Figs. 5, 6, and 7. In Fig. 6, the trajectories $\theta_1(t)$ for various clearances and the variables $g_N(q(t))$ and $\dot{g}_T(q(t))$ are depicted. The normal contact force $R_N(t)$ is also given for the case without friction. Finally, the isolines of the percentage relative error e as given in (16) are plotted and depicted in Fig. 5. The results have been obtained, as indicated in Table 2, for the range of values of restitution coefficient $e_r \in [0.0, 0.9]$. Only one set of simulations for $e_r = 0.0$ is shown in Fig. 6 because changing the restitution coefficient did not change the results significantly in agreement with the results in Fig. 5. The major conclusions are: (i) For the input torque τ_1, the impacts and thus the restitution coefficient e_r

Table 1 Geometric and inertial properties of the crank–rocker four-bar mechanism

Body Nr.	Length [m]	Mass [kg]	Inertia [kg m^2]
1	1.0	1.0	$8.33 \cdot 10^{-2}$
2	4.0	1.0	1.33
3	2.5	1.0	$5.21 \cdot 10^{-1}$
4	3.0	–	–

Table 2 Parameters used in simulations

Nominal bearing radius r_2	0.06 m	Coefficient of restitution e_r	$[0, 0.9]$
Radial clearance c_2 (or c_3)	$[0.0, 5 \cdot 10^{-3}]$ m	Time step h	$1 \cdot 10^{-5}$ s
Coefficient of friction μ	$\{0.0, 0.1\}$	Total time of simulation T	10 s

[5]The name open-loop control means that the torque τ is a function of time only, with no position or velocity feedback.

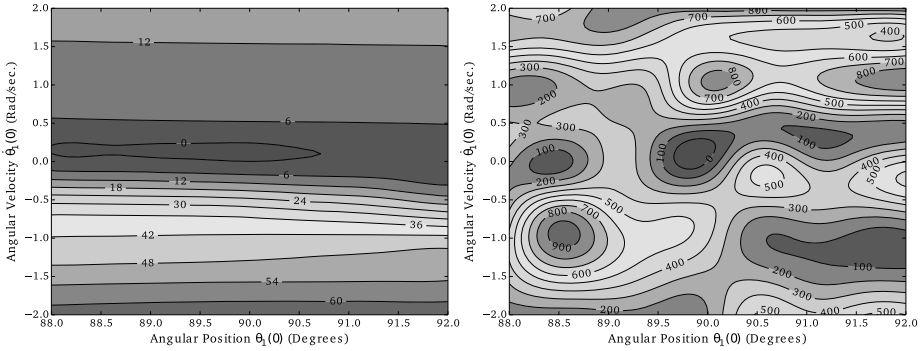

(a) Ideal case, $\tau = \tau_1$. (b) Ideal case, $\tau = \tau_2$.

Fig. 4 Crank-rocker with ideal joints: contour plot of e_0 with $\theta_1(0)$ and $\dot{\theta}_1(0)$

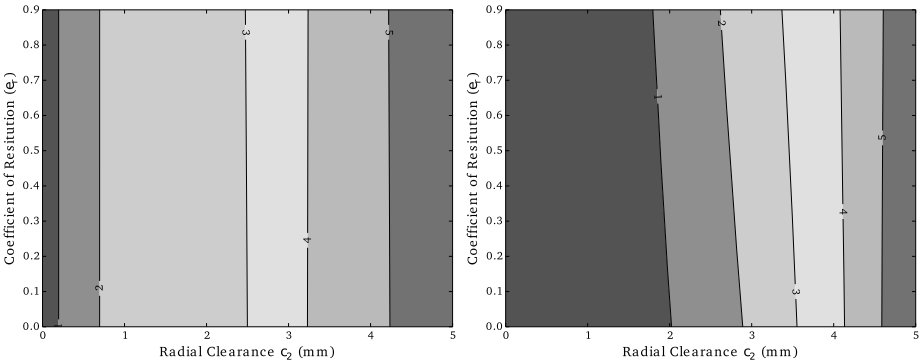

(a) Without friction, $\mu = 0.0$. (b) With friction, $\mu = 0.1$.

Fig. 5 Crank–rocker with clearance in J_2: contour plot of e with c_2 and e_r, τ_1

play a negligible role for fixed clearance (vertical stripes in Fig. 5). This may be attributed to too small values of the preimpact velocities and to a small number of collisions (see the plots of $g_N(q)$ in Figs. 6(a,b,c)). Figures 7 also illustrate that the rebound/contact inside the bearing is confined to small collisions mainly on one side of the bearing, almost independently of e_r. (ii) The maximum values taken by $g_N(q)$ after impacts are most of the time really smaller than the clearance (5 mm in Figs. 6(a,b,c)), in agreement with Fig. 7. (iii) The combined projection scheme in (13) allows us to simulate persistent contact phases without spurious oscillations and with very small drift. This is particularly visible in Figs. 6(a–c) (see $g_N(q(t))$ between the peaks). (iv) For the torque τ_2, the system trajectories (see θ_1 in Fig. 6(c,d)) start deviating from a specific configuration marked as P_1 on the plot, and after this point, the system starts behaving randomly. This is common behavior observed in systems with unilateral constraints and impacts (see, e.g., [91, Figs. 11, 12]; see [16, 47] in the broader context of bifurcation and chaos analysis). (v) Surprisingly enough, the number of impacts with the sinusoidal input torque τ_2 is smaller than that with τ_1 (see $g_N(q)$ in Figs. 6(a,c)). (vi) As seen in Fig. 6(b), the system undergoes few stick/slip transitions in the joint J_2 ($\dot{g}_T(q(t))$ is almost always positive) but with many variations of the tangential

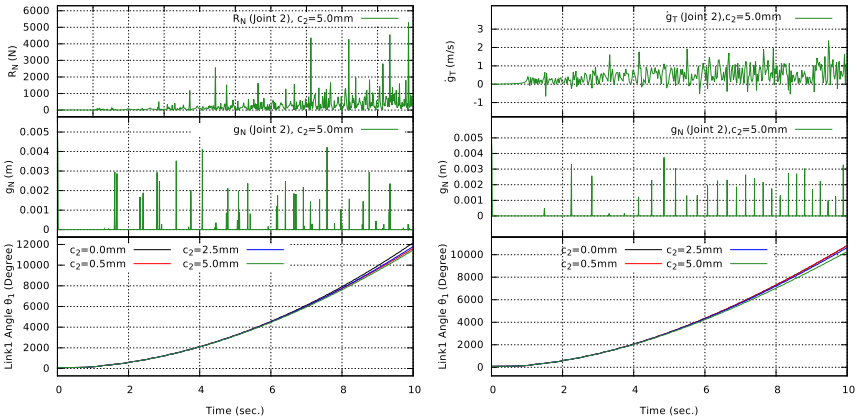

(a) Without friction, $\mu = 0.0$, $\tau = \tau_1$. (b) With friction, $\mu = 0.1$, $\tau = \tau_1$.

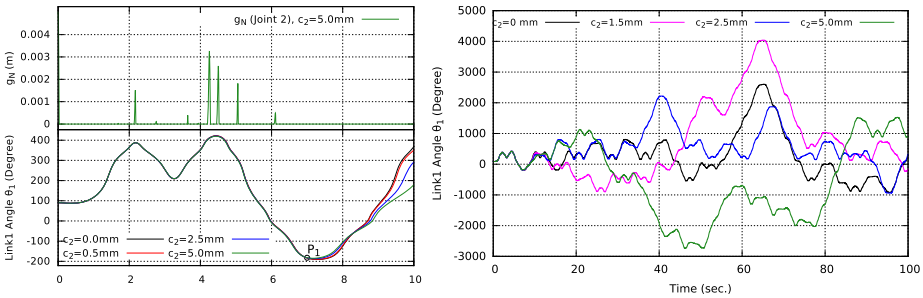

(c) Zoomed on $T \in [0, 10]$s, $\mu = 0.0$, $\tau = \tau_2$. (d) Without friction, $\mu = 0.0$, $\tau = \tau_2$

Fig. 6 Crank–rocker with clearance in J_2: θ_1, g_N, $\dot{g}_T$, and R_N, $e_r = 0.0$

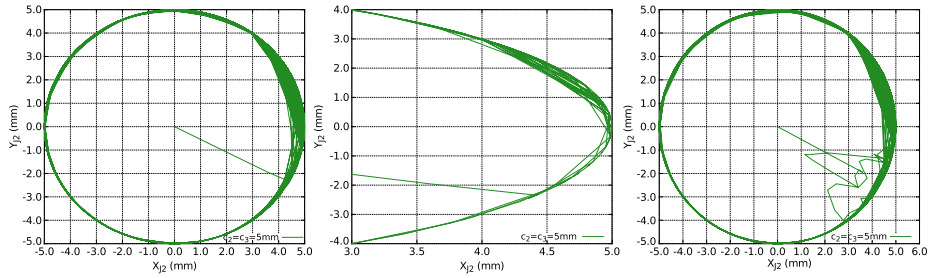

(a) $e_r = 0.0$, $t \in [0, 10]$s. (b) $e_r = 0$, $t \in [0, 3]$s. (c) $e_r = 0.9$, $t \in [0, 10]$s.

Fig. 7 Crank–rocker with clearance in J_2: Journal center locus τ_1

velocity at contact. (vii) For the driving torque τ_1, the presence of small friction does not modify much the dynamical behavior (see Fig. 5 and $g_N(q)$ in Figs. 6(a,b)).

Let us now consider now the crank–rocker mechanism with clearance in joints J_2 and J_3 (see Fig. 3(b)). The isolines of the percentage relative error as given in (16) are plotted for the radial clearances c_2 and c_3. The results for the input torques τ_1 and τ_2 are depicted in Fig. 8(a,b). Some comments arise: (i) In case with torque τ_1, the revolute joint J_3 with clearance c_3 has more influence on the system performance as compared to joint J_2 with

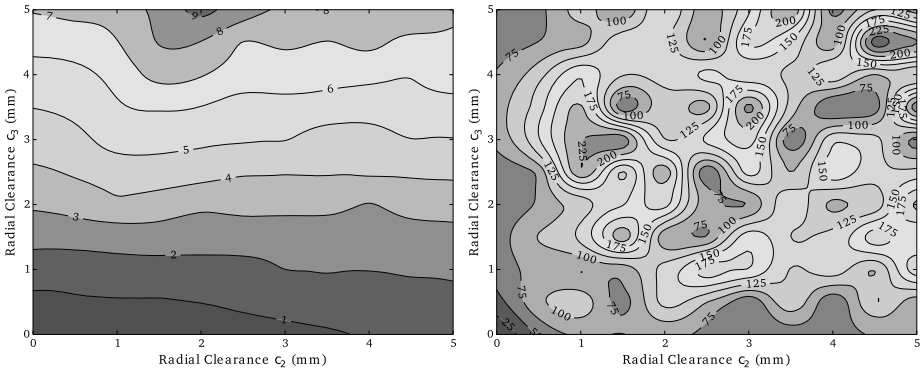

(a) Torque τ_1. (b) Torque τ_2.

Fig. 8 Crank–rocker with clearance in J_2, J_3: contour plot of e with $e_r = 0.0$, $\mu = 0.1$

clearance c_2. This may be attributed to the location of the applied torque. (ii) As expected, the torque τ_2 yields unpredictable behavior with high sensitivity of $e(c_2, c_3)$ (Fig. 8(b)). We infer from Figs. 4(b) and 8(b) that the system actuated with τ_2 is quite sensitive to both initial data and clearances values. The simulations for Fig. 8(b) were led over $[0, 100]$ s in order to capture the long-term behavior of the trajectories (as seen in Figs. 6(c,d) with $c_3 = 0$; trajectories with and without clearance remain close one to each other for τ_2 on the first 10 s).

4 State-feedback control

The main conclusion from the foregoing section is that open-loop controllers may easily lead to unpredictable behavior with high sensitivity to both initial data and clearance values when nonconstant torques are applied. With such a high sensitivity, it is hopeless to try to deduce some universal conclusions on the relative influence of the parameters (e_r, μ, c_2, c_3) on the behavior of the mechanism. It is of interest to investigate if adding a collocated feedback action at joint J_1 may improve the system dynamical behavior when clearances are present (the answer for the no-play case being trivially positive in case of the two nonlinear controllers that guarantee the global exponential Lyapunov stability of the tracking error system). We will in the following consider four types of feedback controllers with increasing complexity: proportional-derivative (PD) plus gravity compensation, with and without desired velocity, feedback linearization, and passivity-based inputs. There are many other types of controllers that have been derived for Lagrangian systems, starting from the basic PD and PID controllers; see, e.g., [5, 14, 41, 42, 74]. In this study, for obvious reasons, we chose to focus ourselves on few of them only.

4.1 Proportional-derivative (PD) controllers

In this section two different types of PD controllers are considered:

$$\tau_3(\theta_1, \dot{\theta}_1, t) = -K_2\dot{\theta}_1 - K_1\big(\theta_1 - \theta_1^d(t)\big) \tag{17}$$

and

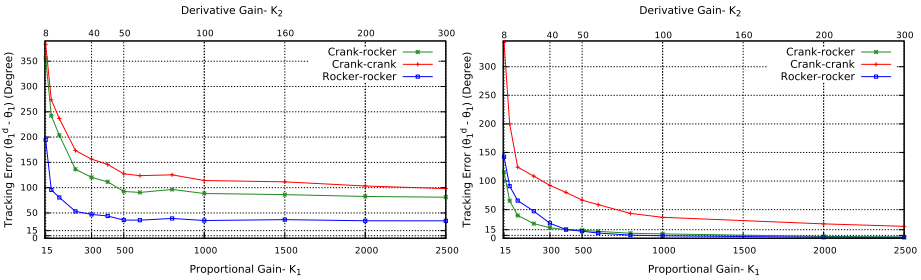

(a) $\tau = \tau_3$. (b) $\tau = \tau_4$.

Fig. 9 PD control: maximum tracking error $\theta_1^d(t) - \theta_1(t)$ vs. controller gains

$$\tau_4(\theta_1, \dot{\theta}_1, t) = -K_2\big(\dot{\theta}_1 - \dot{\theta}_1^d(t)\big) - K_1\big(\theta_1 - \theta_1^d(t)\big), \tag{18}$$

where K_1 and K_2 are positive control gains.

Since system (8) is nonlinear, PD controllers without any kind of feedforward compensation do not a priori guarantee the global asymptotic trajectory tracking of the dynamics (37) with (17) or (18). However, the input τ_4 guarantees the global practical stability [14, Theorem 1]. The choice of the gains may be made by varying the gains and computing the maximum tracking error $\tilde{\theta}_1 \triangleq \theta_1 - \theta_1^d$ in each case, where the desired angle has been chosen as $\theta_1^d(t) = 6.0\sin(0.75\pi t)$ for the crank–rocker and the crank–crank and $\theta_1^d(t) = 3.0 + 2.5\sin(0.75\pi t)$ for the rocker–rocker mechanisms. The maximum tracking errors on [0, 10] s for the crank–rocker, crank–crank, and rocker–rocker four-bar mechanisms are plotted for different values of the control gains K_1 and K_2 in Fig. 9. As expected from [14, Theorem 1], the tracking error decreases as K_1 and K_2 increase and quickly attains an almost constant value for the three mechanisms and both controllers. It is interesting to note that the crank–crank mechanism shows the largest tracking error: this may be due to the fact that the nonlinear torque $N(\theta_1, \dot{\theta}_1)$ in (37) has greater magnitude than for the other two mechanisms. Also, the input τ_4 permits to decrease significantly the tracking error for large enough gains, whereas τ_3 cannot: this demonstrates the usefulness of the feedforward velocity term $K_2\dot{\theta}_1^d$ in (18). For comparison between the various feedback controllers, these gains will also be used for the PD-part of the nonlinear inputs of Sects. 4.2 and 4.3. Thus, they have to satisfy the conditions stated in Appendix C. The choice has been made as $K_1 = 2000$ and $K_2 = 200$ because larger values do not improve the performance as shown in Fig. 9. The constant C in the Lyapunov function (42) can be chosen $C = 10$.

4.1.1 Crank–rocker mechanism

Let us consider a crank–rocker mechanism with clearance in one and two revolute joints (see Figs. 1(a) and 3(a,b)). The Lagrange dynamics is given as in Appendices A.1 and B, respectively, and the system is underactuated with collocated input at joint J_1. The geometric and inertial properties, parameters used for simulation, and initial conditions are given in Sect. 3. The isolines of e in (16), which allow us to compare the cases with and without clearances, are depicted in Fig. 10. They were found to be identical for both τ_3 and τ_4, which shows that the addition of $\dot{\theta}_1^d(t)$ in τ_4 may improve the tracking capabilities, whereas the system precision deterioration is unchanged when clearances are added. Only one set of simulations is shown because changing e_r and μ did not change the results significantly. Comparison of Figs. 8(b) and 10(b) shows a significant discrepancy between open-loop

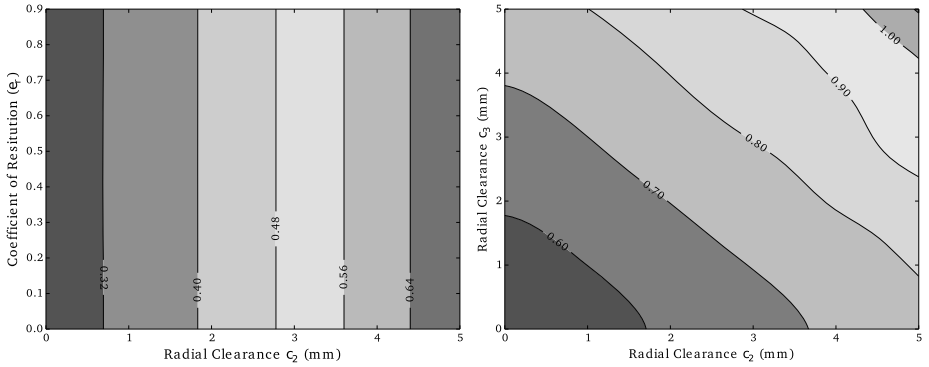

(a) Clearance in J_2: e with c_2 and e_r. (b) Clearance in J_2, J_3: e with c_2 and c_3, $e_r = 0.0$.

Fig. 10 Crank–rocker with PD control: contour plot of e, $\mu \in \{0.0, 0.1\}$, τ_3, and τ_4

Table 3 Geometric and inertial properties of the crank–crank four-bar mechanism

Body Nr.	Length [m]	Mass [kg]	Inertia [kg m^2]
1	1.2	1.0	$1.20 \cdot 10^{-1}$
2	1.2	1.0	$1.20 \cdot 10^{-1}$
3	1.2	1.0	$1.20 \cdot 10^{-1}$
4	1.0	–	–

and state feedback controllers. Actually, the Lyapunov stability of closed-loop systems with state feedback controllers drastically changes their dynamical behavior when clearances are present. It is worth noting that the coefficient of restitution plays no role in the variation of e (see Fig. 10(a)), and there exists a symmetry of the behavior with respect to clearances c_2 and c_3 (see Fig. 10(b)). From Fig. 12 we conclude that, similarly to the case of input τ_1, the journal spends most of the time almost in contact with the bearing, with very small rebounds excepted in few cases where the journal crosses the whole bearing, when the desired trajectory changes its direction (see Fig. 12(b)).

4.1.2 Crank–crank and rocker–rocker mechanisms

Let us consider a crank–crank mechanism with clearance in one and two revolute joints (see Figs. 1(b) and 3(a,b)). The geometric and inertial properties are given in Table 3. The control gains are unchanged. The initial conditions are $\theta_1(0) = 1.658$ rad, $\theta_2(0) = 1.607 \cdot 10^{-4}$ rad, $\theta_3(0) = 1.488$ rad, $\dot{\theta}_1(0) = \dot{\theta}_2(0) = \dot{\theta}_3(0) = 0.0$ rad/s. The control performances are depicted in Figs. 13 and 14. The counterparts of Figs. 10 and 13 for the rocker–rocker mechanism are not shown because they are quite similar to the other two.

4.1.3 Conclusion on PD control

It is visible in Figs. 10 and 13 that: (i) the closed-loop behavior of both PD controllers in (17) and (18) is predictable (the restitution coefficient e_r has negligible influence on e, whereas a symmetric influence of c_2 and c_3 is observed); (ii) the values of e are however much smaller than those for τ_1, indicating that the PD feedback has a significant influence on the systems dynamics in the presence of clearances; (iii) the tracking error is decreasing when τ_4 is used

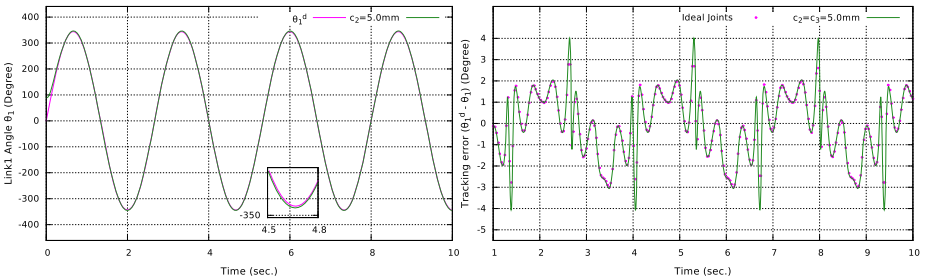

(a) Clearance in one joint J_2, $\theta_1(t)$ and $\theta_1^d(t)$. (b) Tracking error $\tilde{\theta}_1$.

Fig. 11 Crank–rocker with PD control: θ_1 and $\tilde{\theta}_1$ ($e_r = 0.0$, $\mu = 0.1$, $\tau = \tau_4$)

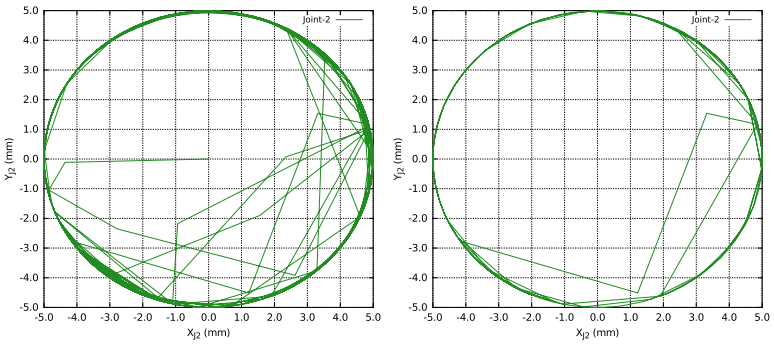

(a) $T \in [0, 10]$s. (b) $T \in [5.4, 8.0]$s

Fig. 12 Crank–rocker with PD control: journal locus inside the bearing

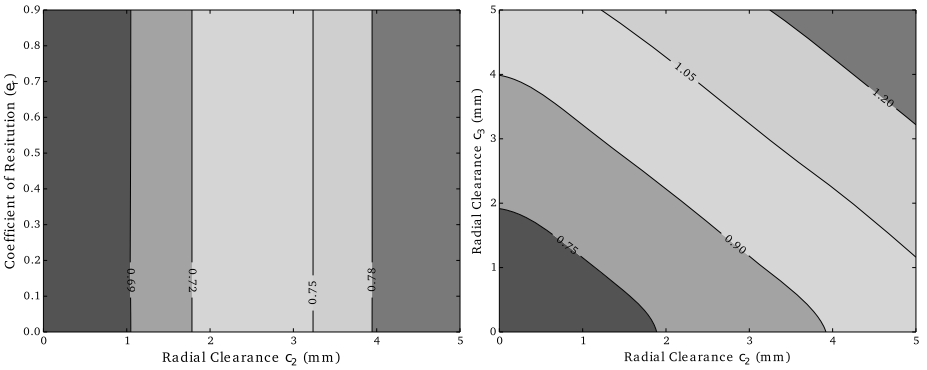

(a) Clearance in J_2: e with c_2 and e_r. (b) Clearance in J_2, J_3: e with c_2 and c_3, $e_r = 0.0$.

Fig. 13 Crank–crank with PD control: contour plot of e, $\mu \in \{0.0, 0.1\}$, τ_3, and τ_4

instead of τ_3 (see Fig. 9); however, this has little influence on e: both controllers gave the same results in Figs. 10 and 13; (iv) from Figs. 9, 10, 11, 13, and 14 it follows that the crank–rocker mechanism provides better performance than the crank–crank one, both for e and the precision at the velocity sign changes (see the zoomed parts in Figs. 11(a) and 14); (v) as

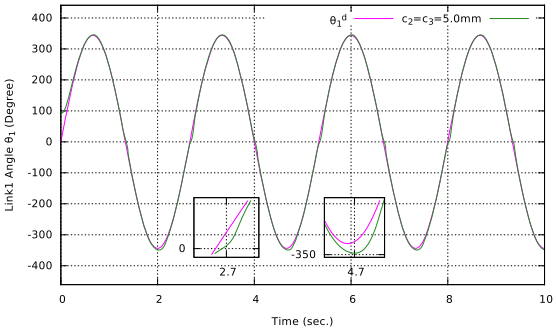

Fig. 14 Crank–crank: PD control with clearance in two joints (J_2, J_3): θ_1 ($e_r = 0.0$, $\mu = 0.1$, $\tau = \tau_4$)

expected, the loss of precision occurs when the desired trajectory changes the direction (see Fig. 14). This motivated some extensions of the PD controllers to improve the accuracy [40].

4.2 State feedback linearization

The smooth part of the dynamic equations of the four-bar mechanism with minimal coordinate is

$$M(\theta_1)\ddot{\theta}_1 + N(\theta_1, \dot{\theta}_1) + g(\theta_1) = \tau_5. \tag{19}$$

Details on how to obtain this minimal coordinate dynamics are given in Appendix A. Let us choose the control torque as

$$\tau_5(\theta_1, \dot{\theta}_1, U) = M(\theta_1)U + N(\theta_1, \dot{\theta}_1) + g(\theta_1). \tag{20}$$

The control law (20) is a simple instance of state feedback linearization. Since $M(\theta_1) > 0$, the closed-loop system (19)–(20) reduces to the double-integrator $\ddot{\theta}_1 = U$. The input U is chosen as the PD controller $U(\theta_1, \dot{\theta}_1, t) = -K_1\theta_1 - K_2\dot{\theta}_1 + \mathbf{r}(t)$. For a given desired trajectory $(\theta_1^d(t), \dot{\theta}_1^d(t))$, we set $\mathbf{r}(t) = \ddot{\theta}_1^d(t) + K_2\dot{\theta}_1^d(t) + K_1\theta_1^d(t)$. Then the tracking error satisfies the closed-loop dynamics

$$\big(\ddot{\theta}_1 - \ddot{\theta}_1^d(t)\big) + K_2\big(\dot{\theta}_1 - \dot{\theta}_1^d(t)\big) + K_1\big(\theta_1 - \theta_1^d(t)\big) = 0, \tag{21}$$

which is globally exponentially stable, with convergence rate depending on the choice of the controller gains. The controller gains have to satisfy the conditions stated in Appendix C. Since the controller may be seen as a PD input with some nonlinearities compensation, the gains will be chosen as for the PD controllers $K_1 = 2000$ and $K_2 = 200$ for comparison.

For brevity, since the results we obtained were quite similar for the three mechanisms, we shall consider in this section a crank–rocker mechanism with clearance in one and two revolute joints (see Figs. 1(a) and 3(a,b)). The desired trajectory of the input link is given as $\theta_1^d = 6.0\sin(0.75\pi t)$. The geometric and inertial properties and the parameters used for simulation are given in Tables 1 and 2, and the initial conditions are as in Sect. 3: $\theta_1(0) = 1.571$ rad, $\theta_2(0) = 0.3533$ rad, $\theta_3(0) = 1.2649$ rad, $\dot{\theta}_1(0) = \dot{\theta}_2 = \dot{\theta}_3(0) = 0.0$ rad/s. The numerical simulations are depicted in Figs. 15, 16, and 17 for the case with clearances in one and two revolute joints. In Fig. 16, the trajectories of the input link $\theta_1(t)$ for various clearances and the Lyapunov function $V(z)$ in (42) are shown. The results have been obtained for different values of $e_r \in [0.0, 0.9]$ and for two different values of $\mu = 0.0$ and $\mu = 0.1$. However, only one set of simulation is shown because changing e_r and μ did not

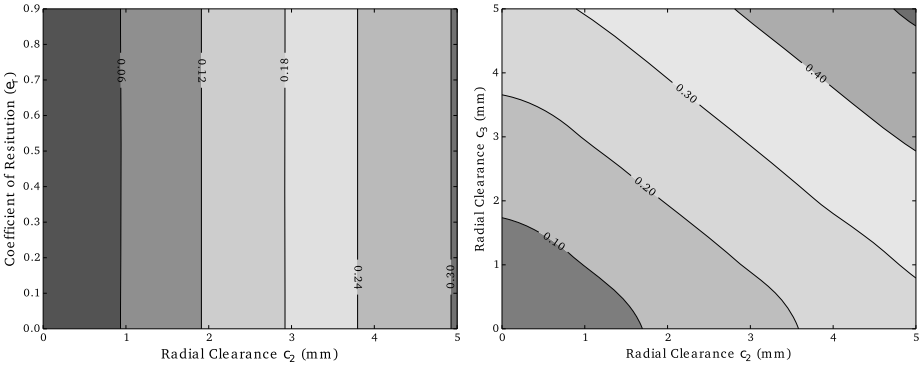

(a) Clearance in J_2: e with c_2 and e_r. (b) Clearance in J_2, J_3: e with c_2 and c_3, $e_r = 0.0$.

Fig. 15 Crank–rocker with state linearization control: contour plot of e, $\mu \in \{0.0, 0.1\}$, $\tau = \tau_5$

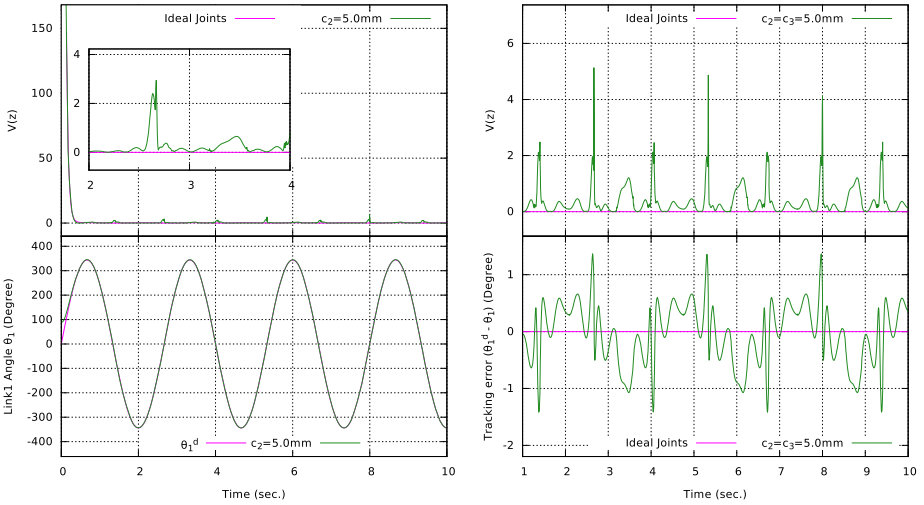

(a) Clearance in one joint J_2. (b) Clearance in two joints J_2 and J_3.

Fig. 16 Crank–rocker with state linearization control: θ_1, $\tilde{\theta}_1$, and $V(z)$ ($e_r = 0.0$, $\mu = 0.1$, $\tau = \tau_5$)

change the results significantly. Some comments arise: (i) Compared to the PD controller, the error e is smaller by a factor 2 for large clearances and by a factor 5 for small clearances (see Figs. 10 and 15). This tends to indicate that the feedback action and the compensation of nonlinearities both have a significant influence on the dynamics with play. (ii) The Lyapunov function remains bounded, but it shows persistent variations after an initial exponential decrease; see Fig. 16: this is due both to the impacts that make the velocity jump and thus induce state reinitializations all along the system motion and to the change of the system dynamics compared to the no-clearance case. Impacts and increasing degrees-of-freedom create a very hard disturbance in the no-clearance-system dynamics, whose effect is not easy to analyze analytically; despite, it should logically decrease as the clearance size c decreases and vanish as $c \to 0$. A discussion about this is proposed in Appendix D. (iii) The tracking error is reduced compared to the PD control since $\tilde{\theta}_1 \in [-4, 4]$ for τ_4 and

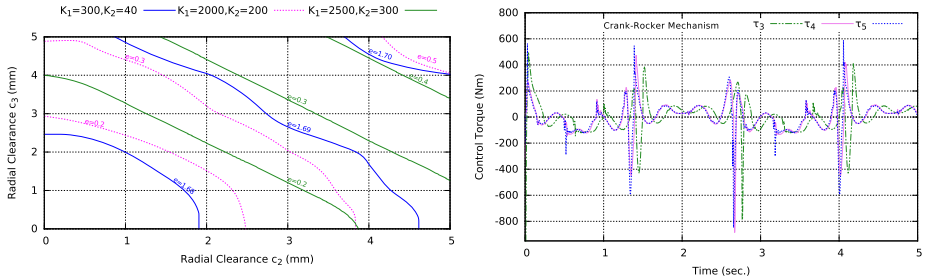

(a) Influence of control gain on e, τ_5.

(b) Comparison: τ_3, τ_4 and τ_5.

Fig. 17 Crank–rocker with state linearization control

$\tilde{\theta}_1 \in [-1.3, 1.3]$ for τ_5 (see Figs. 16(b) and 11(b)). Also, $\tilde{\theta}_1$ with one clearance is smaller than with two clearances; compare $V(z)$ in Figs. 16(a,b). (iv) Increasing the gains K_1 and K_2 allows us to consider larger pairs of clearances (c_2, c_3) for the same error e, as shown in Fig. 17(a). (v) The controllers τ_3, τ_4, and τ_5 possess quite similar shapes and magnitudes, as depicted in Fig. 17(b). However, τ_3 and τ_4 take larger values during the transient period. The absence of feedforward term in τ_3 induces a delay in its reaction to impacts, but τ_4 behaves surprisingly close to the state feedback linearization scheme.

It is visible from Fig. 15 that the three mechanisms, when controlled with a state feedback linearization algorithm, behave in the same way.

Conclusions The feedback linearization control schemes clearly supersede the PD controllers both from the point of view of tracking error reduction (which is a well-known result) and the point of view of the error e reduction. The second set of results (Figs. 10, 13, and 15) means that compensation of the smooth nonlinearities allows us to reduce the closed-loop system sensitivity w.r.t. the presence of clearances.

4.3 Passivity-based control

Passivity-based controllers have become quite popular for the control of nonlinear mechanical systems [10]. Let us investigate now the behavior of the so-called Slotine and Li controller with fixed parameters, which is given in the no-clearance case (37) as

$$\begin{cases} \tau_6(\theta_1, \dot{\theta}_1, t) = M(\theta_1)(\ddot{\theta}_1^d(t) - \Lambda(\dot{\theta}_1 - \dot{\theta}_1^d(t))) \\ \qquad\qquad + C(\theta_1, \dot{\theta}_1)(\dot{\theta}_1^d - \Lambda(\theta_1 - \theta_1^d(t))) + g(\theta_1) - K v, \\ v = (\dot{\theta}_1 - \dot{\theta}_1^d(t)) + \Lambda(\theta_1 - \theta_1^d(t)), \end{cases} \tag{22}$$

where $C(\theta_1, \dot{\theta}_1)\dot{\theta}_1 = N(\theta_1, \dot{\theta}_1)$. The control gain K is similar to the derivative control gain K_2, and the control gain $K\Lambda$ is similar to the proportional control gain K_1. Thus, the control gains are chosen as $K = 200$ and $\Lambda = 10$. The closed-loop dynamics (22), (37) reads as $M(\theta_1)\dot{v} + C(\theta_1, \dot{\theta}_1)v + Kv = 0$ and $\dot{\tilde{\theta}}_1 = -\Lambda\tilde{\theta}_1 + v$.

4.3.1 Collocated control of crank–rocker mechanism

Once again for brevity, we consider in this section a crank–rocker mechanism only. The geometric and inertial properties, the parameters used for simulation, and initial conditions

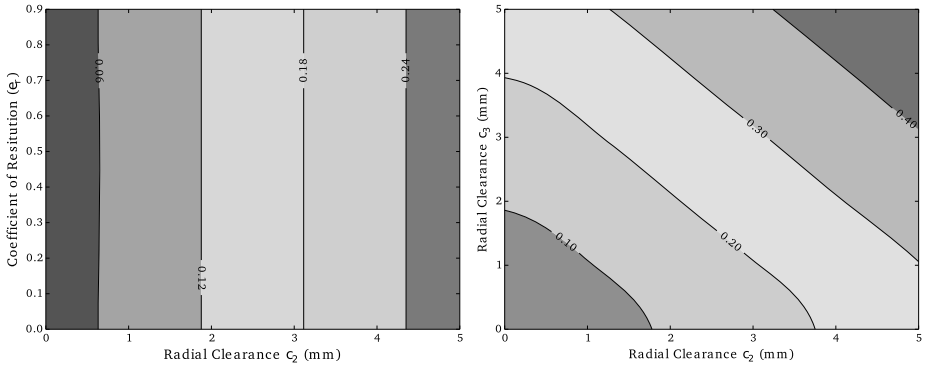

(a) Clearance in J_2: e with c_2 and e_r. (b) Clearance in J_2, J_3: e with c_2 and c_3, $e_r = 0.0$.

Fig. 18 Crank–rocker with passivity-based control: contour plot of e, $\mu \in \{0.0, 0.1\}$, $\tau = \tau_6$

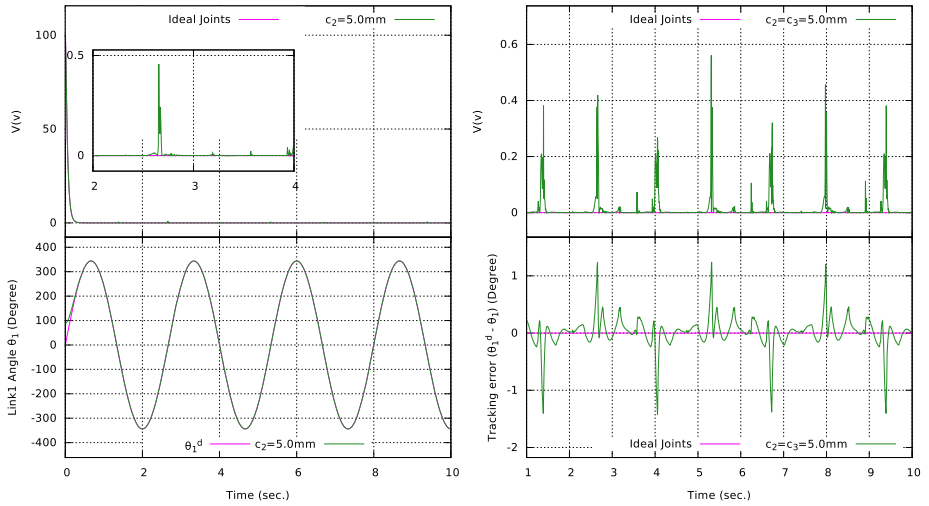

(a) Clearance in one joint J_2. (b) Clearance in two joints J_2 and J_3.

Fig. 19 Crank–rocker with passivity-based control: θ_1, $V(v)$, and $\tilde{\theta}_1$ ($e_r = 0.0$, $\mu = 0.1$, $\tau = \tau_6$)

are as before. The numerical simulations are depicted in Figs. 18, 19, 20, and 21 and in Tables 4 and 5. The results have been obtained for different values of $e_r \in [0.0, 0.9]$ and for two different values of $\mu = 0.0$ and $\mu = 0.1$. However, only one set of simulation is shown because changing e_r and μ did not change the results significantly. Some comments are as follows: (i) Figs. 15 and 18(a,b) show that the passivity-based control algorithm is slightly less sensitive to the clearances than the state linearization one. However, the tracking errors are similar for both controllers (see Figs. 16(b), 19(b) and Tables 4, 5, 7). (ii) For the same precision, the control torque has smaller peaks magnitude when compared to feedback linearization, as shown in Fig. 20 and in Table 4 for various gains. (iii) When the gains are decreased, the maximum tracking error remains almost identical for both controllers, but the passivity-based input maximum value decreases much more than that of the state linearization input (see Table 4). This may be explained by the fact that passivity-based

controllers do not totally compensate the Lagrange dynamics nonlinearities and thus induce less solicitation of the input torque. (iv) The evolution of the Lyapunov-like function $V(v)$ defined in (44) is depicted in Fig. 19(a,b). It shows that the case with one clearance has less impacts than two clearances (similarly to the state linearization in Fig. 16), and it seems that some periodic nonsmooth motion exists in steady-state.[6] The variations of $V(v)$ in Fig. 19 and of $V(z)$ in Fig. 16 demonstrate that the passivity-based controller keeps its Lyapunov function at zero on longer periods than the feedback linearization one. (v) Fig. 21 shows the typical behavior inside a clearance (X_{j2} and Y_{j2} denote the relative position of O_2 inside the bearing): there are few impacts, and the system tends to evolve on the bearing surface. This once again explains why for such desired trajectories, the restitution coefficient does not play a significant role. Comparing Figs. 21 and 12, we infer that compensating for smooth nonlinearities does not modify significantly the journal center motion inside the bearing: most of the time, the system evolves with small values of the gap function (and this, as explained in Appendix D, provides an explanation of the robustness of the closed-loop system). (vi) The influence of the desired trajectory frequency is reported in Table 5. The torques τ_5 and τ_6 show comparable behavior when the frequency is increased. The maximum tracking errors increase in proportion as the frequency of $\theta_1^d(t)$ increases.

Remark 3 (i) The contact/impact model has a great influence on the computed journal center motion inside the bearing [29, Fig. 4.24]. As alluded to above, the model we chose together with the NSCD method of [2] allows us to treat in a clean way the contact phases, avoiding

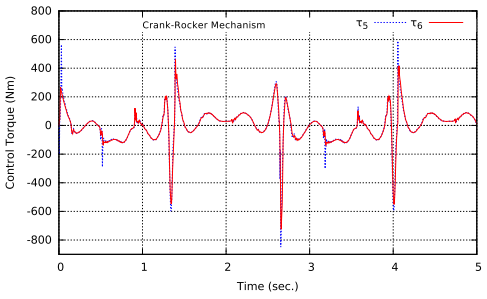

Fig. 20 Crank–rocker: comparison of control torques τ_5 and τ_6

Table 4 Crank–rocker: influence of control gains on the maximum tracking error on [1, 10] s and control torque ($c_2 = c_3 = 5.0$ mm)

Sr. No.	Type of controller	Control gain	Max. tracking error (degree)	Max. control torque (N m)
1	Feedback linearization τ_5	$K_1 = 2000$, $K_2 = 200$	1.34	818.29
	Passivity-based τ_6	$\Lambda = 10$, $K = 200$	1.3	724.45
2	Feedback linearization τ_5	$K_1 = 500$, $K_2 = 100$	2.94	782.59
	Passivity-based τ_6	$\Lambda = 5$, $K = 100$	2.87	604.47
3	Feedback linearization τ_5	$K_1 = 100$, $K_2 = 50$	9.8	697.69
	Passivity-based τ_6	$\Lambda = 2$, $K = 50$	9.21	511.39

[6] In a similar way to the feedback linearization scheme, proving such assertions is far from trivial and is not tackled here; see Appendix D for some discussion about this point.

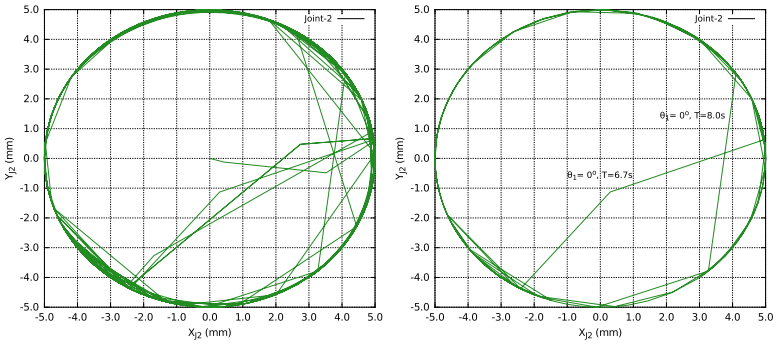

(a) Joint J_2: $T \in [0, 10]$s. (b) Joint J_2: $T \in [5.4, 8.0]$s.

Fig. 21 Crank–rocker with passivity-based control: journal center locus for joint 2

Table 5 Crank–rocker: influence of frequency on the maximum tracking error on [1, 10] s and control torque

Frequency (f)	Max. tracking error (degree)				Max. control torque (N m)			
	Ideal joints		Clearance in J_2, J_3 $c_2 = c_3 = 5.0$ mm		Ideal joints		Clearance in J_2, J_3 $c_2 = c_3 = 5.0$ mm	
	τ_5	τ_6	τ_5	τ_6	τ_5	τ_6	τ_5	τ_6
1.5π	0.004	0.004	3.16	3.2	$2.3 \cdot 10^3$	$2.3 \cdot 10^3$	$3.6 \cdot 10^3$	$2.3 \cdot 10^3$
4.0π	0.005	0.005	5.86	6.0	$1.6 \cdot 10^4$	$1.5 \cdot 10^4$	$1.7 \cdot 10^4$	$1.5 \cdot 10^4$
10.0π	0.014	0.016	11.6	12.4	$9.3 \cdot 10^4$	$9.2 \cdot 10^4$	$9.8 \cdot 10^4$	$9.4 \cdot 10^4$
50.0π	0.176	0.221	126.7	135.9	$1.1 \cdot 10^6$	$8.4 \cdot 10^5$	$1.32 \cdot 10^6$	$9.1 \cdot 10^5$

nonphysical oscillations. Choosing compliant models would yield quite different journal center trajectories.

(ii) A nonlinear feedback controller is considered in [71, Eq. (30)], and applied to a slider-crank mechanism. Contact is modeled with a compliant model. Numerical simulations show possible chaotic behavior. It would be interesting to redo the analysis in this paper on the same slider-crank system to investigate in which way the contact model may change the conclusions and whether or not the above feedback controllers suppress or not the chaos.

4.3.2 Collocated control with clearance in three revolute joints J_2, J_3, and J_4

In this section, a crank–rocker mechanism with clearance in three revolute joints is considered (see Fig. 22). The geometric and inertial properties, the parameters used for simulation, and the initial conditions are as before. The numerical simulations are depicted in Figs. 23, 24, and 25, and in Table 6. The results have been obtained for two different values of the coefficient of restitution, $e_r = 0.0$ and $e_r = 1.0$, and for $\mu = 0.1$. The desired trajectory of the input link is given as $\theta_1^d(t) = 6.0 \sin(0.75\pi t)$.[7] Some comments are as follows: (i) The control torque has larger peak magnitudes when compared to the case with clearance in two revolute joints (compare Figs. 23(a) and 20). (ii) The tracking error does not change significantly due to the additional clearance in the revolute joint J_4 when compared to the

[7]The simulation files may be found on the SICONOS platform website at https://github.com/siconos/siconos/tree/master/examples/Mechanics/FourBarLinkageWith3clearance.

case with clearance in two revolute joints (see Figs. 23(b) and 19(b)). (iii) The evolution of the Lyapunov-like function $V(v)$ for the different values of $e_r = 0.0$ and $e_r = 1.0$ is depicted in Figs. 24(a,b) for $\theta_1^d = 6.0\sin(0.75\pi t)$ and in Fig. 25 for $\theta_1^d = 6.0\sin(50\pi t)$. This shows that at low desired velocities, changing the restitution coefficient from $e_r = 0.0$ to $e_r = 1.0$ does not significantly change the Lyapunov function except at the time instance when the system passes through the angular position of $\theta_1 = 0.0°$ during the clockwise motion (see Fig. 24(a,b)). At higher desired velocities, increasing e_r deteriorates more the performance in terms of position and velocity tracking errors, and in addition tracking errors are much greater (compare Figs. 23, 24, and 25). Similarly, the case with three clearances has larger peaks during impacts when compared to the case with two clearances (see Figs. 24(a)

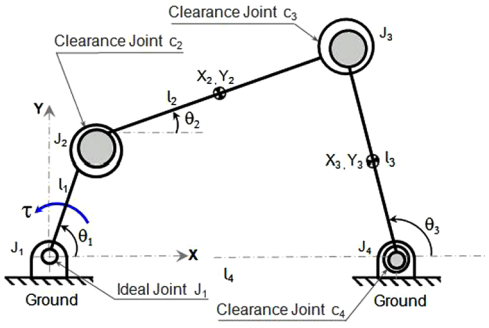

Fig. 22 Four-bar mechanism with clearance in revolute joints J_2, J_3 and J_4

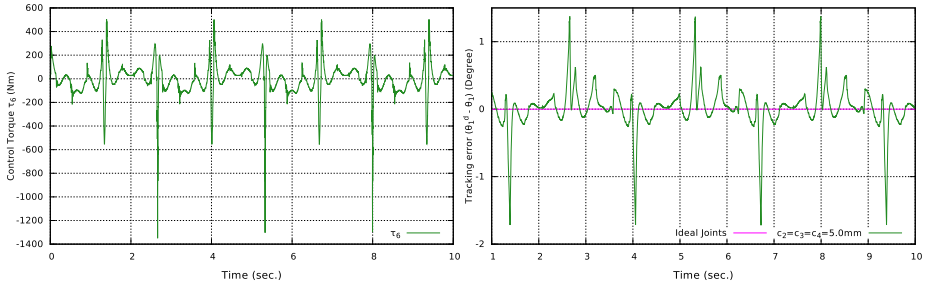

(a) Control torque τ_6, $T \in [0, 10]s$ (b) Tracking error $\tilde{\theta}_1$, $T \in [1, 10]s$

Fig. 23 Crank–rocker mechanism with clearance in joints J_2, J_3, and J_4, $e_r = 0.0$, $\mu = 0.1$, $\tau = \tau_6$

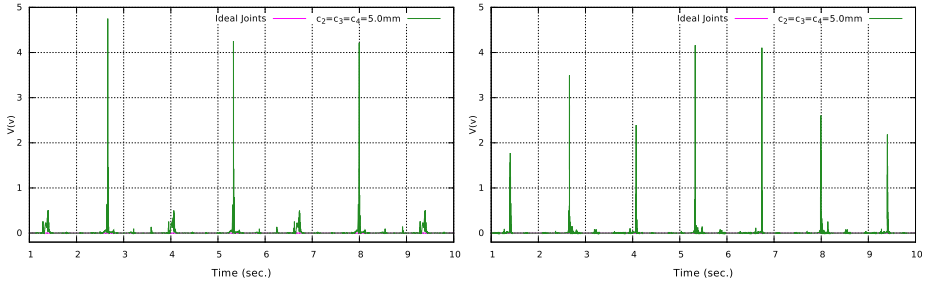

(a) $V(v)$, $e_r = 0.0$. (b) $V(v)$, $e_r = 1.0$.

Fig. 24 Crank–rocker mechanism with clearance in J_2, J_3, and J_4, $\mu = 0.1$, $\tau = \tau_6$, $T \in [1, 10]$ s

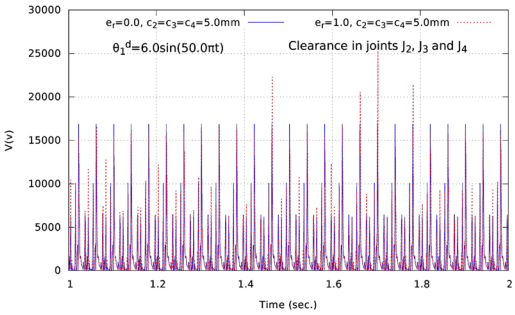

Fig. 25 $V(v)$, $e_r = 0.0$, and $e_r = 1.0$, $\mu = 0.1$, $\tau = \tau_6$, $T \in [1, 2]$ s

Table 6 Crank–rocker: influence of frequency on the maximum tracking error on [1, 10] s and control torque

Frequency (f)	Max. tracking error (degree)	Max. control torque (N m)
	Clearance in joints J_2, J_3, and J_4 $c_2 = c_3 = c_4 = 5.0$ mm	
1.5π	3.50	$3.6 \cdot 10^3$
4.0π	6.49	$1.6 \cdot 10^4$
10.0π	13.10	$9.7 \cdot 10^4$
50.0π	138.49	$1.1 \cdot 10^6$

and 19(b)). (iv) The influence of the desired trajectory frequency is reported in Table 6. The maximum tracking error and the control torque increase in proportion as the frequency of $\theta_1^d(t)$ increases. However, comparing with values in Table 5, we see that adding one more clearance at J_4 does not significantly increase the maximum tracking error nor the maximum control torque.

4.3.3 Noncollocated control of crank–rocker mechanism

All the above results are for the collocated case, that is, we apply the control torque at joint J_1 and measure θ_1 and $\dot{\theta}_1$. It is however possible to use the expressions in (27) in order to obtain the functions $\theta_1(\theta_3)$ and $\dot{\theta}_1(\theta_3, \dot{\theta}_3)$. In the ideal case, using the direct measure of θ_1 and $\dot{\theta}_1$ to compute τ_6, or measuring θ_3 and $\dot{\theta}_3$, then calculating $\theta_1(\theta_3)$ and $\dot{\theta}_1(\theta_3, \dot{\theta}_3)$ and using these expressions to compute a noncollocated input τ_7, we get exactly the same results because $\tau_7(\theta_1(\theta_3), \dot{\theta}_1(\theta_3, \dot{\theta}_3)) = \tau_6(\theta_1, \dot{\theta}_1)$. When clearances are present in joints J_2 and/or J_3, then τ_7 and τ_6 differ since the expressions $\theta_1(\theta_3)$ and $\dot{\theta}_1(\theta_3, \dot{\theta}_3)$ are no longer valid. It is well known that noncollocation deteriorates the control performance[8] and may even destabilize the closed-loop system. Results for the noncollocated input are depicted in Figs. 26 and 27 for $\theta_1^d(t) = 6.0 \sin(0.75\pi t)$. They show a great increase in both e and the tracking error, compared with the collocated control: in Fig. 19, we see that $\tilde{\theta}_1(t) \in [-1, 1]$ degrees, whereas in Fig. 26, $\tilde{\theta}_1(t) \in [-12, 6]$ degrees. In-between the peaks, the tracking errors for τ_7 are also larger than with τ_6.

[8] In [40] the regulation problem is studied –constant desired trajectory– and it is shown that a non-collocated PD controller applied on the simple system of Appendix D, creates stable limit cycles in the closed-loop system.

4.4 Conclusions on Sections 3, 4.1, 4.2, and 4.3

Table 7 summarizes the tracking errors obtained with the above desired trajectories for the torques τ_3, τ_4, τ_5, and τ_6, the three mechanisms, and three cases (no play, one clearance, and two clearances). In view of these data and the above results, the passivity-based controller τ_6 is slightly better than the state linearization τ_5. The two PD controllers, though they allow us to avoid the high sensitivity issues of the open-loop input τ_2, yield too large tracking errors to possess practical interest in case precision is required (though the tracking error is drastically decreased using the velocity feedforward in τ_4). Table 7 summarizes the results obtained for the maximum tracking errors with the four feedback controllers applied to the three mechanisms. Several comments arise, some of which just confirm previous ones: the compensation of smooth nonlinearities drastically improves the accuracy in all cases, and for fixed control gains, the accuracy of PD controllers varies significantly depending on the system, whereas it does not for τ_5 and τ_6; for τ_5 and τ_6, the maximum tracking error doubles when a clearance at J_3 is added. We also see from Figs. 10(b), 13(b), 15(b), and 18(b) that the performance decreases between the no play/play cases and is qualitatively the same for all collocated controllers in the presence of two clearances, whereas a small distortion occurs for the noncollocated input Fig. 27(b). This shows that, at least for the chosen sinusoidal desired trajectories, a good predictability exists in such nonsmooth systems.

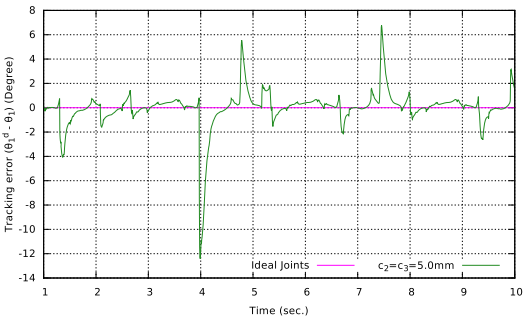

Fig. 26 Crank–rocker with noncollocated passivity-based control τ_7: tracking error

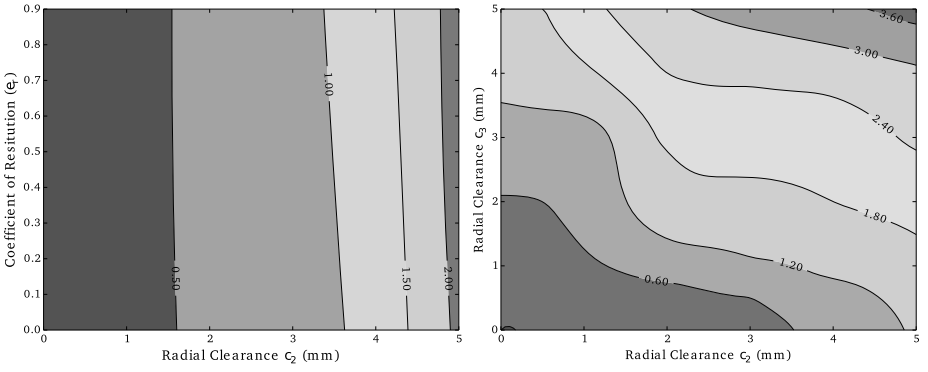

(a) Clearance in J_2: e with c_2 and e_r

(b) Clearance in J_2 and J_3: e with c_2 and c_3, $e_r = 0.0$

Fig. 27 Crank–rocker with noncollocated passivity-based control τ_7: contour plot of e, $\mu \in \{0.0, 0.1\}$, $\tau = \tau_7$

Table 7 Maximum tracking error on [1, 10] s with feedback control, $K_1 = 2000$, $K_2 = 200$, $K = 200$, and $\Lambda = 10$

Four-bar mechanism	Control torque	Maximum tracking error (degrees)		
		Ideal joints	Clearance in joints	
			$c_2 = 3.0$ mm	$c_2 = c_3 = 3.0$ mm
Crank–rocker	τ_3	82.5	84.2	85.2
	τ_4	2.98	5.68	6.68
	τ_5	0.003	0.7	1.2
	τ_6	0.003	0.66	1.12
Crank–crank	τ_3	103.3	105.22	106.92
	τ_4	25.4	27.32	29.02
	τ_5	0.004	0.73	1.31
	τ_6	0.004	0.68	1.22
Rocker–rocker	τ_3	34.57	36.07	37.07
	τ_4	1.79	3.29	4.29
	τ_5	0.003	0.67	1.26
	τ_6	0.003	0.61	1.19

5 Conclusions

A general methodology for modeling and simulation of multiple revolute joints with clearance in planar four-bar mechanisms is presented and discussed in this work and used to compare the robustness properties of several classical trajectory tracking feedback controllers (proportional-derivative, state linearization, and passivity-based control algorithms) with respect to such hard disturbances. The methodology is based on the nonsmooth dynamical approach, in which the interactions of the colliding bodies (journal and bearing) are modeled with unilateral constraints, restitution coefficients, and Coulomb's friction. The combined projected Moreau–Jean event–capturing (time-stepping) scheme derived in [2] is used to solve numerically the contact-impact problem. It improves significantly the drift issue at the position level and allows us to simulate persistent contact phases without spurious contact force and acceleration oscillations. It is worth noting that the contact/impact models may be easily enhanced (taking into account static and dynamic friction, Stribeck effects, micro-displacements during sticking modes, velocity-dependent coefficients of restitution, etc.) while using the same dynamical and numerical framework. The major conclusions of this work are that collocated state feedback control improves drastically the system dynamics (in the sense that trajectories of the clearance-free system and trajectories of the system with clearances are close one to each other) and that the nonlinear controllers significantly improve the precision. Also, the influence of the restitution (loss of kinetic energy at collisions) is negligible in our tested examples, whereas the clearances induce a symmetric behavior. The three-dimensional case should deserve attention since it has considerable practical significance. In this setting, cylindrical contact/impact models could be incorporated. The studied nonlinear feedback controllers could be enhanced using ideas from [40] to augment the precision of the closed-loop system. Finally, structural optimization may also be used to improve the closed-loop system overall performance and decrease the control input magnitude and the effects of collisions.

Appendix A: Lagrangian formulation of four-bar mechanisms with reduced coordinates

A four-bar mechanism is the simplest form of closed-chain linkage and possesses one degree-of-freedom. The loop-closure constraints in the x and y coordinates are given as

$$l_4 + l_3\cos\theta_3 - l_2\cos\theta_2 - l_1\cos\theta_1 = 0, \tag{23}$$

$$l_3\sin\theta_3 - l_2\sin\theta_2 - l_1\sin\theta_1 = 0. \tag{24}$$

From (23) and (24) we can express θ_2 and θ_3 in terms of θ_1. After some mathematical manipulations, we get

$$c_1(\theta_1)\sin(\theta_3) + c_2(\theta_1)\cos(\theta_3) + c_3(\theta_1) = 0, \tag{25}$$

where $c_1(\theta_1) = -2l_1l_3\sin\theta_1, c_2(\theta_1) = -2l_3(l_4 - l_1\sin\theta_1), c_3(\theta_1) = l_4^2 + l_1^2 - l_2^2 + l_3^2 - 2l_1l_4\cos\theta_1$. Equation (25) can be solved in closed form as

$$p = \tan\frac{\theta_3}{2}, \qquad \sin\theta_3 = \frac{2p}{1+p^2}, \qquad \cos\theta_3 = \frac{1-p^2}{1+p^2}. \tag{26}$$

From (25) and (26) we have $(c_3 - c_2)p^2 + (2c_1)p + (c_2 + c_3) = 0$, whose solution is $p = \frac{-c_1 \pm \sqrt{c_1^2 + c_2^2 - c_3^2}}{c_3 - c_2}$. Then we obtain:

$$\theta_3(\theta_1) = 2\arctan 2\Big(-c_1 \pm \sqrt{c_1^2 + c_2^2 - c_3^2}, c_3 - c_2\Big), \tag{27}$$

$$\theta_2(\theta_1, \theta_3) = \arctan 2(-l_1\sin\theta_1 + l_3\sin\theta_3, l_3\cos\theta_3 - l_1\cos\theta_1), \tag{28}$$

where the mapping $\arctan 2(\cdot,\cdot)$ is defined by

$$\arctan 2(y,x) = \begin{cases} \arctan\frac{y}{x}, & x > 0, \\ \arctan\frac{y}{x} + \pi, & y \geq 0, x < 0, \\ \arctan\frac{y}{x} - \pi, & y < 0, x < 0, \\ +\frac{\pi}{2}, & y > 0, x = 0, \\ -\frac{\pi}{2}, & y < 0, x = 0, \\ \text{undefined}, & y = x = 0. \end{cases} \tag{29}$$

Differentiating (23) and (24) with respect to time yields:

$$l_1\sin\theta_1\dot{\theta}_1 + l_2\sin\theta_2\dot{\theta}_2 - l_3\sin\theta_3\dot{\theta}_3 = 0, \tag{30}$$

$$-l_1\cos\theta_1\dot{\theta}_1 - l_2\cos\theta_2\dot{\theta}_2 + l_3\cos\theta_3\dot{\theta}_3 = 0. \tag{31}$$

We can determine the velocities $\dot{\theta}_2$ and $\dot{\theta}_3$ in terms of $\dot{\theta}_1$ as

$$\dot{\theta}_2 = \frac{\partial\theta_2}{\partial\theta_1}\dot{\theta}_1 = \frac{l_1\sin(\theta_3 - \theta_1)}{l_2\sin(\theta_2 - \theta_3)}\dot{\theta}_1, \tag{32}$$

$$\dot{\theta}_3 = \frac{\partial\theta_3}{\partial\theta_1}\dot{\theta}_1 = \frac{l_1\sin(\theta_2 - \theta_1)}{l_2\sin(\theta_2 - \theta_3)}\dot{\theta}_1. \tag{33}$$

The dynamical system is formulated from the Euler–Lagrange equations:

$$\frac{d}{dt}\left(\frac{\partial L(\theta_1,\dot{\theta}_1)}{\partial \dot{\theta}_1}\right)-\left(\frac{\partial L(\theta_1,\dot{\theta}_1)}{\partial \theta_1}\right)=\tau, \tag{34}$$

$$L(\theta_1,\dot{\theta}_1)=T(\theta_1,\dot{\theta}_1)-V(\theta_1), \tag{35}$$

where $L(\theta_1,\dot{\theta}_1)\in\mathbb{R}$ is the Lagrangian function, $T(\theta_1,\dot{\theta}_1)=\frac{1}{2}\dot{\theta}_1^T M(\theta_1)\dot{\theta}_1$ is the total kinetic energy, $V(\theta_1)$ is the total potential energy of the system, and τ is the external torque. The Lagrangian function is given as

$$\begin{aligned}L(\theta_1,\theta_2,\theta_3,\dot{\theta}_1,\dot{\theta}_2,\dot{\theta}_3)=&\big(T_1(\theta_1,\dot{\theta}_1)+T_2(\theta_1,\theta_2,\dot{\theta}_2,\dot{\theta}_2)+T_3(\theta_3,\dot{\theta}_3)\big)\\&-\big(V_1(\theta_1)+V_2(\theta_1,\theta_2)+V_3(\theta_3)\big),\end{aligned} \tag{36}$$

where $T_1=0.25m_1l_1^2\dot{\theta}_1^2+0.5I_1\dot{\theta}_1^2$, $V_1=0.5m_1l_1\mathbf{g}\sin\theta_1$, $V_2=m_2\mathbf{g}(l_1\sin\theta_1+0.5l_2\sin\theta_2)$, $V_3=0.5m_3l_3\mathbf{g}\sin\theta_3$, $T_2=0.5m_2(l_1^2\dot{\theta}_1^2+0.5l_2^2\dot{\theta}_2^2+l_1l_2\cos(\theta_1-\theta_2)\dot{\theta}_1\dot{\theta}_2)+0.5I_2\dot{\theta}_2^2$, $T_3=0.25m_3l_3^2\dot{\theta}_3^2+0.5I_3\dot{\theta}_3^2$, and $\mathbf{g}$ is the gravitational acceleration. From (34) we infer the dynamics

$$M(\theta_1)\frac{d\dot{\theta}_1}{dt}+N(\theta_1,\dot{\theta}_1)+g(\theta_1)=\tau, \tag{37}$$

where:

$$M(\theta_1)=2\big(J_1+J_2A_1^2+J_3A_2^2+0.5m_2l_1l_2\cos(\theta_1-\theta_2)\big),$$

$$g(\theta_1)=-(C_1+A_1C_2+A_2C_3),$$

$$N(\theta_1,\dot{\theta}_1)=\big(2J_2A_1A_{19}+2J_3A_2A_{20}+A_4\big(A_3A_{19}+A_1(A_{11}+A_1A_{12})\big)\big)\dot{\theta}_1^2,$$

$$A_1=\frac{l_1\sin(\theta_3-\theta_1)}{l_2\sin(\theta_2-\theta_3)},\qquad A_2=\frac{l_1\sin(\theta_2-\theta_1)}{l_2\sin(\theta_2-\theta_3)},\qquad A_3=\cos(\theta_1-\theta_2),$$

$$A_4=0.5m_2l_1l_2,\qquad A_5=\frac{\partial A_1}{\partial\theta_1}=\frac{-l_1\cos(\theta_3-\theta_1)}{l_2\sin(\theta_2-\theta_3)},$$

$$A_6=\frac{\partial A_1}{\partial\theta_2}=\frac{-l_1\sin(\theta_3-\theta_1)\cos(\theta_2-\theta_3)}{l_2\sin^2(\theta_2-\theta_3)},\qquad A_7=\frac{\partial A_1}{\partial\theta_3}=\frac{-2l_1\sin(\theta_2-\theta_1)}{-l_2+l_2\cos(2\theta_2-2\theta_3)},$$

$$A_8=\frac{\partial A_2}{\partial\theta_1}=\frac{-l_1\cos(\theta_2-\theta_1)}{l_3\sin(\theta_2-\theta_3)},\qquad A_9=\frac{\partial A_2}{\partial\theta_2}=\frac{2l_1\sin(\theta_3-\theta_1)}{-l_3+l_3\cos(2\theta_2-2\theta_3)},$$

$$A_{10}=\frac{\partial A_2}{\partial\theta_3}=\frac{l_1\sin(\theta_2-\theta_1)\cos(\theta_2-\theta_3)}{l_3\sin^2(\theta_2-\theta_3)},\qquad A_{11}=\frac{\partial A_3}{\partial\theta_1}=\sin(\theta_2-\theta_1),$$

$$A_{12}=\frac{\partial A_3}{\partial\theta_1}=-\sin(\theta_2-\theta_1),\qquad A_{19}=A_5+A_1A_6+A_2A_7,$$

$$A_{20}=A_8+A_1A_9+A_2A_{10},\qquad J_1=0.5\big(0.33m_1l_1^2+m_2l_1^2\big),\qquad J_2=0.17m_2l_2^2,$$

$$J_3=0.17m_3l_3^2,\qquad C_1=-(0.5m_1l_1+m_2l_1)\mathbf{g}\cos\theta_1,\qquad C_2=-0.5m_2l_2\mathbf{g}\cos\theta_2,$$

$$C_3=-0.5m_3l_3\mathbf{g}\cos\theta_3.$$

A.1 Four-bar mechanism with clearance at joint J_2

A four-bar mechanism with clearance in one revolute joint (see Fig. 3(a)) possesses three degrees of freedom. The Lagrange dynamics in (12) is given as follows:

$$M(q) = \begin{bmatrix} \mathcal{J}_1 & 0 & 0 \\ 0 & \mathcal{J}_2 & 0.5\mathcal{N}_2 \\ 0 & 0.5\mathcal{N}_2 & \mathcal{J}_3 \end{bmatrix}, \qquad G(q) = \begin{bmatrix} G_{11} & G_{12} & G_{13} \\ G_{21} & G_{22} & G_{23} \end{bmatrix}, \tag{38}$$

$$C(q,\dot{q}) = \begin{bmatrix} 0 \\ 0.5\mathcal{N}_1\dot{\theta}_3^2 \\ 0.5\mathcal{N}_1\dot{\theta}_2^2 \end{bmatrix}, \qquad g(q) = \begin{bmatrix} 0.5m_1F_1 \\ 0.5m_2F_2 \\ (m_2+0.5m_3)F_3 \end{bmatrix}, \tag{39}$$

where: $\mathcal{J}_1 = I_1 + 0.25m_1l_1^2$, $\mathcal{J}_2 = I_2 + 0.25m_2l_2^2$, $\mathcal{J}_3 = I_3 + m_2l_3^2 + 0.25m_3l_3^2$, $\mathcal{N}_1 = -m_2l_2l_3\sin(\theta_2-\theta_3)$, $\mathcal{N}_2 = -m_2l_2l_3\cos(\theta_2-\theta_3)$, $F_1 = \mathbf{g}l_1\cos\theta_1$, $F_2 = -\mathbf{g}l_2\cos\theta_2$, $F_3 = \mathbf{g}l_3\cos\theta_3$, $E = \sqrt{E_x^2+E_y^2}$, $E_x = -l_4 - l_3\cos\theta_3 + l_2\cos\theta_1 + l_1\cos\theta_1$, $E_y = -l_3\sin\theta_3 + l_2\sin\theta_2 + l_1\sin\theta_1$, $G_{11} = (l_1\sin\theta_1E_x - l_1\cos\theta_1E_y)/E$, $G_{21} = ((-l_1\sin\theta_1E_y - l_1\cos\theta_1E_x)/E) + r_1$, $G_{12} = (l_2\sin\theta_2E_x - l_2\cos\theta_2E_y)/E$, $G_{13} = (-l_3\sin\theta_3E_x + l_3\cos\theta_3E_y)/E$, $G_{22} = ((-l_2\sin\theta_2E_y - l_2\cos\theta_2E_x)/E) - r_2$, $G_{23} = (l_3\sin\theta_3E_y + l_3\cos\theta_3E_x)/E$.

Appendix B: Four-bar mechanism with clearances at joints J_2 and J_3

A four-bar mechanism with clearance in two revolute joints (see Fig. 3(b)) possesses 5 degrees of freedom. The unconstrained dynamics is that of three independent bodies and is given by

$$M(q) = \begin{bmatrix} I_1+(0.25m_1)l_1^2 & 0 & 0 & 0 & 0 \\ 0 & I_2 & 0 & 0 & 0 \\ 0 & 0 & I_3+(0.25m_3)l_3^2 & 0 & 0 \\ 0 & 0 & 0 & m_2 & 0 \\ 0 & 0 & 0 & 0 & m_2 \end{bmatrix},$$

$$g(q) = \begin{bmatrix} 0.5m_1\mathbf{g}l_1\cos\theta_1 \\ 0 \\ 0.5m_3\mathbf{g}l_3\cos\theta_3 \\ 0 \\ m_2\mathbf{g} \end{bmatrix}, \qquad B = \begin{bmatrix} 1 \\ 0 \\ 0 \\ 0 \\ 0 \end{bmatrix}, \tag{40}$$

$$N(q,\dot{q}) = \begin{bmatrix} 0 \\ 0 \\ 0 \\ 0 \\ 0 \end{bmatrix}, \qquad G_1(q) = \begin{bmatrix} G_{11} & G_{12} & 0 & G_{14} & G_{15} \\ G_{21} & G_{22} & 0 & G_{24} & G_{25} \end{bmatrix},$$

$$G_2(q) = \begin{bmatrix} 0 & \mathcal{G}_{12} & \mathcal{G}_{13} & \mathcal{G}_{14} & \mathcal{G}_{15} \\ 0 & \mathcal{G}_{22} & \mathcal{G}_{23} & \mathcal{G}_{24} & \mathcal{G}_{25} \end{bmatrix}, \tag{41}$$

where:

$$G_{11} = (-X_2 l_1 \sin\theta_1 + 0.5 l_1 l_2 \sin(\theta_1 - \theta_2) + Y_3 l_1 \cos\theta_1) Cl_1,$$

$$G_{21} = ((X_2 l_1 \cos\theta_1 - 0.5 l_1 l_2 \cos(\theta_1 - \theta_2) + Y_3 l_1 \sin\theta_1 - l_1^2)/Cl_1) + r_1,$$

$$G_{12} = (-0.5 X_2 l_2 \sin\theta_2 - 0.5 l_1 l_2 \sin(\theta_1 - \theta_2) + 0.5 Y_2 l_2 \cos\theta_2)/V_1,$$

$$G_{22} = ((0.5 X_2 l_2 \cos\theta_2 - 0.5 l_1 l_2 \cos(\theta_1 - \theta_2) + 0.5 Y_2 l_2 \sin\theta_2 - 0.25 l_2^2)/Cl_1) - r_2,$$

$$G_{14} = (-X_2 + l_1 \cos\theta_1 + 0.5 l_2 \cos\theta_2)/Cl_1,$$

$$G_{15} = (-Y_2 + l_1 \sin\theta_1 + 0.5 l_2 \sin\theta_2)/Cl_1,$$

$$G_{24} = (X_2 - l_1 \sin\theta_1 - 0.5 l_2 \sin\theta_2)/Cl_1,$$

$$G_{25} = -(Y_2 - l_1 \cos\theta_1 - 0.5 l_2 \cos\theta_2)/Cl_1,$$

$$\mathcal{G}_{12} = (-0.5 l_4 l_2 \sin\theta_2 - 0.5 l_2 l_3 \sin(\theta_2 - \theta_3) + 0.5 X_2 l_2 \sin\theta_1 - 0.5 Y_2 l_2 \cos\theta_2)/Cl_2,$$

$$\mathcal{G}_{13} = (l_4 l_3 \sin\theta_3 + 0.5 l_2 l_3 \sin(\theta_2 - \theta_3) - X_2 l_3 \sin\theta_3 + Y_2 l_3 \cos\theta_3)/Cl_2,$$

$$\mathcal{G}_{22} = ((0.5 l_4 l_2 \cos\theta_2 - 0.5 l_2 l_3 \sin(\theta_2 - \theta_3) - 0.5 X_2 l_2 \cos\theta_1 + 0.5 Y_2 l_2 \cos\theta_2 - 0.2.5 l_2^2)/Cl_2) + r_3,$$

$$\mathcal{G}_{23} = ((-l_4 l_3 \cos\theta_3 + 0.5 l_2 l_3 \cos(\theta_2 - \theta_3) + X_2 l_3 \cos\theta_3 + Y_2 l_3 \sin\theta_3 - l_3^2)/Cl_2) - r_4,$$

$$\mathcal{G}_{14} = (-X_2 + l_4 + l_3 \cos\theta_3 - 0.5 l_2 \cos\theta_2)/Cl_2,$$

$$\mathcal{G}_{24} = (Y_2 - l_3 \sin\theta_3 + 0.5 l_2 \sin\theta_2)/Cl_2,$$

$$\mathcal{G}_{15} = (-Y_2 + l_3 \sin\theta_3 - 0.5 l_2 \sin\theta_2)/Cl_2,$$

$$\mathcal{G}_{25} = (-X_2 + l_4 + l_3 \cos\theta_3 - 0.5 l_2 \cos\theta_2)/Cl_2,$$

$$Cl_1 = \sqrt{(X_2 - 0.5 l_2 \cos\theta_2 - l_1 \cos\theta_1)^2 + (Y_2 - 0.5 l_2 \sin\theta_2 - l_1 \sin\theta_1)^2},$$

$$Cl_2 = \sqrt{(-l_4 - l_3 \cos\theta_3 + 0.5 l_2 \cos\theta_2 + X_2)^2 + (-l_3 \sin\theta_3 + 0.5 l_2 \sin\theta_2 + Y_2)^2}.$$

Appendix C: Lyapunov functions

The candidate Lyapunov function for the closed-loop system in (21) is given as

$$\mathbf{V}(z) = \frac{1}{2}\left(\dot{\tilde{\theta}}_1^2 + K_1 \tilde{\theta}_1^2 + C\tilde{\theta}_1 \dot{\tilde{\theta}}_1\right) = \frac{1}{2} z^T P z, \tag{42}$$

where $P = \begin{bmatrix} K_1 & 0.5C \\ 0.5C & 1 \end{bmatrix}$, the position and velocity tracking errors are $\tilde{\theta}_1 \triangleq (\theta_1 - \theta_1^d)$ and $\dot{\tilde{\theta}}_1 \triangleq (\dot{\theta}_1 - \dot{\theta}_1^d)$, $z = (\tilde{\theta}_1, \dot{\tilde{\theta}}_1)^T$. Differentiating the Lyapunov function along the closed-loop system trajectories gives

$$\begin{aligned} \dot{\mathbf{V}}(z) &= \dot{\tilde{\theta}}_1 (K_2 \dot{\tilde{\theta}}_1 - K_1 \tilde{\theta}_1) + K_1 \tilde{\theta}_1 \dot{\tilde{\theta}}_1 + C\dot{\tilde{\theta}}_1^2 + C\tilde{\theta}_1(-K_2 \dot{\tilde{\theta}}_1 - K_1 \tilde{\theta}_1) \\ &= k_2 \dot{\tilde{\theta}}_1^2 + C\dot{\tilde{\theta}}_1^2 - CK_2 \tilde{\theta}_1 \dot{\tilde{\theta}}_1 - CK_1 \tilde{\theta}_1^2 = -z^T Q z, \end{aligned} \tag{43}$$

where $Q = \begin{bmatrix} K_2 - C & 0.5CK_2 \\ 0.5CK_2 & CK_1 \end{bmatrix}$. The matrices Q and P are positive definite if and only if the gains satisfy $0 < C < \frac{K_1 K_2}{K_1 + 0.25K_2}$, $K_2 > C$, $K_1 > \frac{C^2}{4}$. The closed-loop dynamics with the passivity-based controller in (22) admits the following Lyapunov-like function [10, p. 404]

$$V(v) = \frac{1}{2} v^T M(\theta_1) v \quad \text{with } \dot{V}(v) = -v^T K v \tag{44}$$

It allows us to prove that in the ideal no-clearance case, all trajectories of (22), (37) are bounded and the tracking errors globally asymptotically converge to zero.

Appendix D: Trajectory tracking: stability analysis with a clearance

Let us provide a short analysis that demonstrates why clearances induce serious additional difficulty in the closed-loop stability analysis, but which also provides a possible explanation of the robustness of the state feedback controllers studied in this article. In order to simplify the presentation, let us consider a one-degree-of-freedom system with mass $m > 0$ and coordinate q_1, acted upon by a control force τ: $m\ddot{q}_1(t) = \tau(t)$. The passivity-based controller is $\tau = \tau_6 = m(\ddot{q}_d(t) - \Lambda\dot{\tilde{q}}_1(t)) - Kv$ with $v = \dot{\tilde{q}}_1 + \Lambda\tilde{q}_1$, and the closed-loop system is $m\dot{v}(t) + Kv(t) = 0$ with $V(v) = \frac{1}{2}mv^2$. Let us assume now that there is a clearance between the actuated mass m_1 with coordinate q_1, and the remaining part m_2 with coordinate q_2, with $m = m_1 + m_2$ (a one-degree-of-freedom prismatic joint with clearance). The two unilateral constraints are $g_N^1(q_1, q_2) = q_1 - q_2 + \epsilon + l \geq 0$ and $g_N^2(q_1, q_2) = q_2 - q_1 - l \geq 0$ for some $l > 0$ and the clearance size $\epsilon \geq 0$. The complementarity conditions are $0 \leq \lambda_1 \perp g_N^1(q_1, q_2) \geq 0$ and $0 \leq \lambda_2 \perp g_N^2(q_1, q_2) \geq 0$, where λ_1 and λ_2 are the contact forces. The dynamics becomes $m_1\ddot{q}_1(t) = \tau(t) + \lambda_1 - \lambda_2$, $m_2\ddot{q}_2(t) = \lambda_2 - \lambda_1$. Newton's impact law applied at both constraints (which cannot be active at the same time since $g_N^1(q_1, q_2) = 0 \Rightarrow g_N^2(q_1, q_2) = \epsilon$ and $g_N^2(q_1, q_2) = 0 \Rightarrow g_N^1(q_1, q_2) = \epsilon$) is $\dot{q}_1(t^+) - \dot{q}_2(t^+) = -e_1(\dot{q}_1(t^-) - \dot{q}_2(t^-))$ if $g_N^1(q_1(t), q_2(t)) = 0$ and $\dot{q}_2(t^+) - \dot{q}_1(t^+) = -e_2(\dot{q}_2(t^-) - \dot{q}_1(t^-))$ if $g_N^2(q_1(t), q_2(t)) = 0$. When $\epsilon = 0$, ($g_N^1(q_1, q_2) \geq 0$ and $g_N^2(q_1, q_2) \geq 0$) implies that $q_1 = q_2 - l$. These three ingredients (Lagrange dynamics, complementarity conditions, and Newton's impact law) allow us to recast our system into (12), where $U_N^i = \dot{g}_N^i = \nabla g_N^i(q)^T \dot{q}$, $i = 1, 2$.

The clearance introduces a disturbance in the dynamics of the controlled mass through the contact forces λ_1 and λ_2, as well as a parameter change since $m_1 \neq m$.[9] Let us now look at the term $\lambda_1 - \lambda_2$. During noncontact phases of motion, $\lambda_1 = \lambda_2 = 0$. During persistent contact with one of the constraints boundary, the multipliers are solutions of the so-called *contact linear complementarity problem* (CLCP) [9]: $0 \leq \lambda_1(t) \perp \ddot{g}_N^1(t) = \ddot{q}_1(t) - \ddot{q}_2(t) = \frac{1}{m_1}(\tau(t) + \lambda_1(t) - \lambda_2(t)) - \frac{1}{m_2}(\lambda_2(t) - \lambda_1(t)) \geq 0$ and $0 \leq \lambda_2(t) \perp \ddot{g}_N^2(t) = \ddot{q}_2(t) - \ddot{q}_1(t) = \frac{1}{m_2}(\lambda_2(t) - \lambda_1(t)) - \frac{1}{m_1}(\tau(t) + \lambda_1(t) - \lambda_2(t)) \geq 0$. As we noticed before, the two constraints cannot be active at the same time, and thus the CLCP reduces to two independent LCPs $0 \leq \lambda_1(t) \perp \frac{1}{m_1}\tau(t) + (\frac{1}{m_1} + \frac{1}{m_2})\lambda_1(t) \geq 0$ and $0 \leq \lambda_2(t) \perp (\frac{1}{m_1} + \frac{1}{m_2})\lambda_2(t) - \frac{1}{m_1}\tau(t) \geq 0$, which are easily solvable by inspection as

$$\lambda_1(t) = \begin{cases} 0 & \text{if } \tau(t) \geq 0, \\ \frac{-m_2\tau(t)}{m_1+m_2} & \text{if } \tau(t) < 0, \end{cases} \quad \text{and} \quad \lambda_2(t) = \begin{cases} 0 & \text{if } \tau(t) < 0, \\ \frac{m_2\tau(t)}{m_1+m_2} & \text{if } \tau(t) \geq 0. \end{cases}$$

[9] If we make the analogy with the four-bar mechanism, this may be the difference between $M(\theta_1)$ in (37) and the first diagonal entry of $M(q)$ in (40).

The transitions from contact to noncontact phase of motion are ruled by the two CLCPs: when a multiplier vanishes, we have to compute the sign of $\frac{d^2}{dt^2} g_N^i(q_1(t), q_2(t))$ to infer detachment or persisting contact. We therefore obtain the following closed-loop dynamics outside impact times:

$$m_1 \ddot{q}_1(t) = \begin{cases} \begin{cases} \text{(a) } \frac{m_1}{m}\tau(t) & \text{if } \tau(t) < 0, \\ \text{(b) } 0 & \text{if } \tau(t) \geq 0, \end{cases} & \text{if } g_N^1(q_1, q_2) = 0 \ \big(\Rightarrow g_N^2(q_1, q_2) = \epsilon\big), \\ \begin{cases} \text{(c) } \frac{m_1}{m}\tau(t) & \text{if } \tau(t) > 0, \\ \text{(d) } 0 & \text{if } \tau(t) \leq 0, \end{cases} & \text{if } g_N^2(q_1, q_2) = 0 \ \big(\Rightarrow g_N^1(q_1, q_2) = \epsilon\big), \\ \text{(e) } \tau(t) & \text{if } g_N^1(q_1, q_2) > 0 \quad \text{and} \quad g_N^2(q_1, q_2) > 0. \end{cases} \tag{45}$$

We see from (45) that contrary to the no-clearance case, the sign of the controller plays a significant role in the switching dynamics. Going a step further, we may rewrite the controlled modes (a), (c), and (e) as

$$\begin{cases} \text{(a) } m\dot{v}(t) + Kv(t) = 0 & \text{if } m(\ddot{q}_d(t) - \Lambda\dot{\tilde{q}}_1(t)) - Kv(t) < 0 \\ & \quad \text{and} \quad g_N^1(q_1(t), q_2(t)) = 0, \\ \text{(c) } m\dot{v}(t) + Kv(t) = 0 & \text{if } m(\ddot{q}_d(t) - \Lambda\dot{\tilde{q}}_1(t)) - Kv(t) > 0 \\ & \quad \text{and} \quad g_N^2(q_1(t), q_2(t)) = 0, \\ \text{(e) } m\dot{v}(t) + \frac{m}{m_1}Kv(t) = \frac{m}{m_1}(m - m_1)(\ddot{q}_d(t) - \Lambda\dot{\tilde{q}}_1(t)) & \\ \qquad \text{if } g_N^1(q_1(t), q_2(t)) > 0 & \\ \qquad \text{and} \quad g_N^2(q_1(t), q_2(t)) > 0. & \end{cases} \tag{46}$$

It is worth noting that the Lyapunov-like function $V(v)$ exponentially decreases during the contact modes (a) and (c); however, its variation during mode (e) is not clear. Moreover, the transition from mode (e) to either mode (a) or mode (c) usually involves impacts. Let us compute the variation of $V(v)$ at an impact time t, taking into account that positions are continuous (as well as $q_d(\cdot)$, $\dot{q}_d(\cdot)$, and $\ddot{q}_d(\cdot)$ in our control framework):

$$\begin{aligned} V\big(t^+\big) - V\big(t^-\big) &= \frac{1}{2}mv\big(t^+\big)^2 - \frac{1}{2}mv\big(t^-\big)^2 \\ &= \frac{1}{2}m\big\{\big(\dot{q}_1\big(t^+\big) + \dot{q}_1\big(t^-\big) - 2\dot{q}_d(t)\big)\big(\dot{q}_1\big(t^+\big) - \dot{q}_1\big(t^-\big)\big) \\ &\quad + \Lambda\tilde{q}_1\big(\dot{q}_1\big(t^+\big) - \dot{q}_1\big(t^-\big)\big)\big\}. \end{aligned} \tag{47}$$

Using the impact dynamics and the restitution law, we further obtain $\dot{q}_1(t^+) = \frac{m_2}{m_1}((1 + e_1)\dot{q}_2(t^-) + (\frac{m_1}{m_2} - e_1)\dot{q}_1(t^-))$. It seems hopeless to take advantage of the kinetic energy loss at impacts to infer the sign of $V(t^+) - V(t^-)$ in (47). This is because $V(v)$ is close to the kinetic energy of the no-play system but is quite different from the total kinetic energy of the system with play. We can nevertheless state that if the system spends enough time in modes (a) and (c), then the possible increase of $V(v)$ during mode (e) and at impacts may be compensated so that globally $V(v)$ remains bounded. In control theory, one speaks of suitable dwell times, which are in our case both state-triggered and time-dependent (through the presence of the desired trajectory in the switching conditions) as shown in (46). Intuitively, it follows from the switching conditions that if the tracking errors are small compared to the desired acceleration $\ddot{q}_d(t)$, then the switching function $m(\ddot{q}_d(t) - \Lambda\dot{\tilde{q}}_1(t)) - Kv(t)$ may keep its sign and prevent detachment. The numerical simulations presented in this paper seem to confirm that, at least for a certain range of desired trajectories and clearances, this

does happen in the four-bar mechanism; see Figs. 12 and 21 and Table 5, which shows that indeed the performance degrades as the system speed increases. We see also from Figs. 19 and 16 that the Lyapunov functions vary much less in case of one clearance, as expected.

Starting from (45), it is easy to redo the same analysis for the feedback linearization controller in (20). The switching function in (46) becomes $-K_1\tilde{q}_1(t) - K_2\dot{\tilde{q}}_1(t) + \ddot{q}_d(t)$; thus, similar conclusions may be drawn.

This brief analysis suggests that properties like asymptotic stability will have to be relaxed to boundedness or practical stability of the error system when classical trajectory tracking controllers are applied without taking clearances into account in their design. The stability frameworks proposed in [8, 11, 12, 33, 51, 54, 55] apply mainly to fully actuated systems, starting the design and analysis from a tracking controller that guarantees the stability of the unconstrained system (all unilateral constraints satisfy $g_N^i(q) > 0$): the control philosophy for systems with clearances adopted in this paper is quite different since we start with a controller for the reduced-order system when $g_N^i(q) = 0$ for all i. The control of underactuated mechanical systems with impacts and unilateral constraints has been tackled in [13, 40, 53] using very specific dead-beat feedback controllers. In particular, the PD control of the above simple system is thoroughly studied in [40], where improvements that allow one to track triangular desired trajectories are proposed. Another path may reside in using an output (position) feedback controller as in [50] designed for the unconstrained system (all $g_N^i(q) > 0$) whose Lyapunov function is close to the system kinetic energy and is therefore more amenable for its analysis at impact times. This however requires the measure of the whole vector q (which in many cases seems to be a reasonable option) and also the actuation of more than one joint to assure that the system is fully actuated.

References

1. Abadie, M.: Dynamic simulation of rigid bodies: modelling of frictional contact. In: Brogliato, B. (ed.) Impacts in Mechanical Systems: Analysis and Modelling. Lecture Notes in Physics (LNP), vol. 551, pp. 61–144. Springer, Berlin (2000)
2. Acary, V.: Projected event–capturing time-stepping schemes for nonsmooth mechanical systems with unilateral contact and Coulomb's friction. Comput. Methods Appl. Mech. Eng. **256**, 224–250 (2013)
3. Acary, V.: Energy conservation and dissipation properties of time-integration methods for nonsmooth elastodynamics with contact. J. Appl. Math. Mech./Z. Angew. Math. Mech. (2015). doi:10.1002/zamm.201400231
4. Acary, V., Brogliato, B.: Numerical Methods for Nonsmooth Dynamical Systems. Applications in Mechanics and Electronics. Lecture Notes in Applied and Computational Mechanics, vol. 35. Springer, Berlin (2008). xxi, 525 p.
5. Angeli, D.: Input-to-state stability of PD-controlled robotic systems. Automatica **35**, 1285–1290 (1999)
6. Ballard, P.: The dynamics of discrete mechanical systems with perfect unilateral constraints. Arch. Ration. Mech. Anal. **154**, 199–274 (2000)
7. Ballard, P., Basseville, S.: Existence and uniqueness for frictional unilateral contact with Coulomb friction: a model problem. ESAIM: M2AN Modél. Math. Anal. Numér. **39**, 59–75 (2005)
8. Bourgeot, J.-M., Brogliato, B.: Tracking control of Lagrangian complementarity systems. Int. J. Bifurc. Chaos **15**(6), 1839–1866 (2005). Special issue on Nonsmooth Dynamical Systems
9. Brogliato, B.: Nonsmooth Mechanics: Models, Dynamics and Control. Communications and Control Engineering, 3rd edn. Springer, London (2016)
10. Brogliato, B., Lozano, R., Maschke, B., Egeland, O.: Dissipative Systems Analysis and Control: Theory and Applications, 2nd edn. Springer, Berlin (2007)
11. Brogliato, B., Niculescu, S., Orhant, P.: On the control of finite dimensional mechanical systems with unilateral constraints. IEEE Trans. Autom. Control **42**(2), 200–215 (1997)
12. Brogliato, B., Niculescu, S.-I., Monteiro-Marques, M.: On tracking control of a class of complementary-slackness hybrid mechanical systems. Syst. Control Lett. **39**(4), 255–266 (2000)
13. Brogliato, B., Zavala-Rio, A.: On the control of complementary-slackness mechanical juggling systems. IEEE Trans. Autom. Control **45**(2), 235–246 (2000)

14. Chen, Q., Chen, H., Wang, Y., Woo, P.Y.: Global stability analysis of some trajectory-tracking control schemes of robotic manipulators. J. Robot. Syst. **18**(2), 69–75 (2001)
15. Cole, M.O.T., Wongratanaphisan, T., Pongvuthithum, R., Fakkaew, W.: Controller design for flexible structure vibration suppression with robustness to contacts. Automatica **44**, 2876–2883 (2008)
16. di Bernardo, M., Budd, C.J., Champneys, A.R., Kowalczyk, P.: Piecewise Smooth Dynamical Systems: Theory and Applications. Applied Mathematical Sciences, vol. 163. Springer, London (2008)
17. Duarte, F.B., Tenreiro Machado, J.: Describing function of two masses with backlash. Nonlinear Dyn. **56**, 409–413 (2009)
18. Dubowsky, S., Freudenstein, F.: Dynamic analysis of mechanical systems with clearances—part 1: formation of dynamic model. J. Eng. Ind. **93**, 305–309 (1971)
19. Dubowsky, S., Freudenstein, F.: Dynamic analysis of mechanical systems with clearances—part 2: dynamic response. J. Eng. Ind. **93**, 310–316 (1971)
20. Dzonou, R., Monteiro Marques, M.D.P.: A sweeping process approach to inelastic contact problems with general inertia operators. Eur. J. Mech. A, Solids **26**(3), 474–490 (2007)
21. Dzonou, R., Monteiro Marques, M.D.P., Paoli, L.: A convergence result for a vibro-impact problem with a general inertia operator. Nonlinear Dyn. **58**(1–2), 361–384 (2009)
22. Earles, S.W.E., Wu, C.L.S.: Motion analysis of a rigid link mechanism with clearance at a bearing using Lagrangian mechanics and digital computation. In: Mechanisms (Proceedings, Institution of Mechanical Engineers), London, vol. 22, pp. 83–89 (1973)
23. Erkaya, S., Uzmay, I.: Determining link parameters using genetic algorithm in mechanisms with joint clearance. Mech. Mach. Theory **44**(1), 222–234 (2009)
24. Erkaya, S., Uzmay, I.: Investigation on effect of joint clearance on dynamics of four-bar mechanism. Nonlinear Dyn. **58**, 179–198 (2009)
25. Erkaya, S., Uzmay, I.: Balancing planar mechanisms having imperfect joints using neural network-genetic algorithm (NN-GA) approach. In: Zhang, D., Wei, B. (eds.) Dynamic Balancing of Mechanisms and Synthesizing, pp. 299–317. Springer, Berlin (2016)
26. Farahanchi, F., Shaw, S.W.: Chaotic and periodic dynamics of a slider–crank mechanism with slider clearance. J. Sound Vib. **177**(3), 307–324 (1994)
27. Flores, P.: A parametric study on the dynamic response of planar multibody systems with multiple clearance joints. Nonlinear Dyn. **61**(4), 633–653 (2010)
28. Flores, P., Ambrósio, J.: Revolute joints with clearance in multibody systems. Comput. Struct. **82**(17), 1359–1369 (2004)
29. Flores, P., Ambrosio, J., Pimenta Claro, J.C., Lankarani, H.M.: Kinematics and Dynamics of Multibody Systems with Imperfect Joints. Lecture Notes in Applied and Computational Mechanics, vol. 34. Springer, Heidelberg (2008)
30. Flores, P., Koshy, C.S., Lankarani, H.M., Ambrosio, J., Claro, J.C.P.: Numerical and experimental investigation on multibody systems with revolute clearance joints. Nonlinear Dyn. **65**, 383–398 (2011)
31. Flores, P., Leine, R., Glocker, C.: Modeling and analysis of planar rigid multibody systems with translational clearance joints based on the non-smooth dynamics approach. Multibody Syst. Dyn. **23**, 165–190 (2010)
32. Funabashi, H., Ogawa, K., Horie, M.: A dynamic analysis of mechanisms with clearances. Bull. JSME **21**(161), 1652–1659 (1978)
33. Galeani, S., Menini, L., Potini, A., Tornambé, A.: Trajectory tracking for a particle in elliptical billiards. Int. J. Control **81**(2), 189–213 (2008)
34. Glocker, C.: Set-Valued Force Laws. Lecture Notes in Applied Mechanics, vol. 1. Springer, Berlin (2001)
35. Gummer, A., Sauer, B.: Modeling planar slider–crank mechanisms with clearance joints in RecurDyn. Multibody Syst. Dyn. **31**, 127–145 (2014)
36. Haines, R.S.: Survey: 2-dimensional motion and impact at revolute joints. Mech. Mach. Theory **15**(5), 361–370 (1980)
37. Horie, M., Funabashi, H., Ogawa, K., Abe, H.: Dynamic characteristics of planar link mechanisms with clearances: conditions of separation occurrence between pairing elements. Bull. JSME **29**(252), 1888–1894 (1986)
38. Jean, M.: The non-smooth contact dynamics method. Comput. Methods Appl. Mech. Eng. **177**(3), 235–257 (1999)
39. Jean, M., Moreau, J.J.: Dynamics in the presence of unilateral contacts and dry friction: a numerical approach. In: del Piero, G., Maceri, F. (eds.) Unilateral Problems in Structural Analysis II. CISM Courses and Lectures, vol. number 304, pp. 151–196. Springer, Berlin (1987)
40. Mata Jimenez, M., Brogliato, B.: Analysis of PD and nonlinear control of mechanical systems with dynamic backlash. J. Vib. Control **9**(1), 119–156 (2003)

41. Kelly, R., Carelli, R.: A class of nonlinear PD-type controllers for robot manipulators. J. Robot. Syst. **13**(12), 793–802 (1996)
42. Kikuuwe, R.: Alternative proofs of four stability properties of rigid-link manipulators under PID position control. Robotica **31**(1), 113–122 (2012)
43. Koshy, C.S., Flores, P., Lankarani, H.M.: Study of the effect of contact force model on the dynamic response of mechanical systems with dry clearance joints: computational and experimental approaches. Nonlinear Dyn. **73**, 325–338 (2013)
44. Krinner, A., Thümmel, T.: Non-smooth behaviour of a linkage mechanism with revolute clearance joints. In: New Advances in Mechanisms, Transmissions and Applications, pp. 233–241. Springer, Berlin (2014)
45. Lagerberg, A.: A literature survey on control of automotive powertrains with backlash. Control and Automation Laboratory, Chalmers University of Technology, Göteborg, Sweden, R013/2001
46. Lagerberg, A., Egardt, B.: Backlash estimation with application to automotive powertrains. IEEE Trans. Control Syst. Technol. **15**(3), 483–493 (2007)
47. Leine, R.I., Nijmeijer, H.: Dynamics and Bifurcations of Non-Smooth Mechanical Systems. Lecture Notes in Applied and Computational Mechanics, vol. 18. Springer, Berlin (2004)
48. Li, X., Ding, X., Chirikjian, G.S.: Analysis of angular-error uncertainty in planar multiple-loop structures with joint clearances. Mech. Mach. Theory **91**, 69–85 (2015)
49. Liu, C., Tian, Q., Hu, H.: Dynamics and control of a spatial rigid-flexible multibody system with multiple cylindrical clearance joints. Mech. Mach. Theory **52**, 106–129 (2012)
50. Loria, A.: Observers are unnecessary for output-feedback control of Lagrangian systems. IEEE Trans. Autom. Control **61**(4), 905–920 (2016). doi:10.1109/TAC.2015.2446831
51. Menini, L., Tornambé, A.: Asymptotic tracking of periodic trajectories for a simple mechanical system subject to nonsmooth impacts. IEEE Trans. Autom. Control **46**(7), 1122–1126 (2001)
52. Menini, L., Tornambé, A.: State estimation of (otherwise unobservable) linear mechanical systems through the use of non-smooth impacts: the case of two mating gears. Automatica **38**, 1823–1826 (2002)
53. Menini, L., Tornambé, A.: Control of (otherwise) uncontrollable linear mechanical systems through non-smooth impacts. Syst. Control Lett. **49**(4), 311–322 (2003)
54. Morarescu, C.-I., Brogliato, B.: Passivity-based switching control of flexible-joint complementarity mechanical systems. Automatica **46**(1), 160–166 (2010)
55. Morarescu, C.-I., Brogliato, B.: Trajectory tracking control of multiconstraint complementarity Lagrangian systems. IEEE Trans. Autom. Control **55**(6), 1300–1313 (2010)
56. Moreau, J.J.: Standard inelastic shocks and the dynamics of unilateral constraints. In: CISM Courses and Lectures, vol. 288, pp. 173–221. Springer, Berlin (1985). Preprint 84-2, February 1984, Laboratoire de Mécanique Générale des Milieux Continus, Université des Sciences et Techniques du Languedoc, France
57. Moreau, J.J.: Unilateral contact and dry friction in finite freedom dynamics. In: Moreau, J.J., Panagiotopoulos, P.D. (eds.) Nonsmooth Mechanics and Applications. CISM, vol. 302, pp. 1–82. Spinger, Berlin (1988)
58. Moreau, J.J.: Some numerical methods in multibody dynamics: application to granular materials. Eur. J. Mech. A, Solids **13**, 93–114 (1994)
59. Moreau, J.J.: Numerical aspects of the sweeping process. Comput. Methods Appl. Mech. Eng. **177**, 329–349 (1999)
60. Müller, A.: Internal preload control of redundantly actuated parallel manipulators—its application to backlash avoiding control. IEEE Trans. Robot. **21**(4), 668–677 (2005)
61. Nordin, M., Galic, J., Gutman, P.O.: New models for backlash and gear play. Int. J. Adapt. Control Signal Process. **1**, 9–63 (1997)
62. Nordin, M., Gutman, P.O.: Controlling mechanical systems with backlash—a survey. Automatica **38**, 1633–1649 (2002)
63. Olyaei, A.A., Ghazavi, M.R.: Stabilizing slider–crank mechanism with clearance joints. Mech. Mach. Theory **53**, 17–29 (2012)
64. Olyaei, A.A., Ghazavi, M.Z.: Stabilizing slider–crank mechanism with clearance joints. Mech. Mach. Theory **53**, 17–29 (2012)
65. Garcia Orden, J.C.: Analysis of joint clearances in multibody systems. Multibody Syst. Dyn. **13**, 401–420 (2005)
66. Paoli, L.: A proximal-like method for a class of second order measure-differential inclusions describing vibro-impact problems. J. Differ. Equ. **250**(1), 476–514 (2011)
67. Pennestri, E., Valentini, P.P., Vita, L.: Multibody dynamics simulation of planar linkages with Dahl friction. Multibody Syst. Dyn. **17**, 321–347 (2007)
68. Pereira, C., Ramalho, A., Ambrosio, J.: An enhanced cylindrical contact force model. Multibody Syst. Dyn. **35**(3), 277–298 (2015). doi:10.1007/s11044-015-9463-x

69. Pfeiffer, F., Glocker, C.: Multibody Dynamics with Unilateral Contacts. Non-linear Dynamics. Wiley, New York (1996)
70. Potra, F.R., Anitescu, M., Gavrea, B., Trinkle, J.C.: Linearly implicit trapezoidal method for integrating stiff multibody dynamics with contact, joints, and friction. Int. J. Numer. Methods Eng. **66**(7), 1079–1124 (2005)
71. Rahmanian, S., Ghazavi, M.R.: Bifurcation in planar slider–crank mechanism with revolute clearance joint. Mech. Mach. Theory **91**, 86–101 (2015)
72. Ravn, P.: A continuous analysis method for planar multibody systems with joint clearance. Multibody Syst. Dyn. **2**(1), 1–24 (1998)
73. Rhee, J., Akay, A.: Dynamic response of a revolute joint with clearance. Mech. Mach. Theory **31**(1), 121–134 (1996)
74. Santibanez, V., Kelly, R.: PD control with feedforward compensation for robot manipulators: analysis and experimentation. Robotica **19**(1), 11–19 (2001)
75. Seneviratne, L.D., Earles, S.W.E.: Chaotic behaviour exhibited during contact loss in a clearance joint of a four-bar mechanism. Mech. Mach. Theory **27**(3), 307–321 (1992)
76. Stewart, D.E.: Convergence of a time-stepping scheme for rigid-body dynamics and resolution of Painlevé's problem. Arch. Ration. Mech. Anal. **145**(3), 215–260 (1998)
77. Stewart, D.E., Trinkle, J.C.: An implicit time-stepping scheme for rigid body dynamics with inelastic collisions and Coulomb friction. Int. J. Numer. Methods Eng. **39**, 2673–2691 (1996)
78. Studer, C.: Numerics of Unilateral Contacts and Friction—Modeling and Numerical Time Integration in Non-Smooth Dynamics. Lecture Notes in Applied and Computational Mechanics, vol. 47. Springer, Berlin (2009)
79. Thümmel, T., Funk, K.: Multibody modelling of linkage mechanisms including friction, clearance and impact. In: Proceedings of the 10th World Congress on the Theory of Machines and Mechanisms in Oulu, June 20 to 24, vol. 4, pp. 1387–1392. Oulu University Press, Finland (1999)
80. Tang, Y., Chang, Z., Dong, X., Hu, Y., Yu, Z.: Nonlinear dynamics and analysis of a four-bar linkage with clearance. Front. Mech. Eng. **8**(2), 160–168 (2013)
81. Tao, G., Kokotovic, P.V.: Adaptive control of systems with backlash. Automatica **29**(2), 323–335 (1993)
82. Tao, G., Kokotovic, P.V.: Adaptive control of plants with unknown hystereses. IEEE Trans. Autom. Control **40**(2), 200–212 (1995)
83. Thümmel, T.: Experimentelle Mechanismendynamik: Messung, Modellierung, Simulation, Verifikation, Interpretation und Beeinflussung typischer Schwingungsphänomene an einem Mechanismenprüfstand. PhD thesis, München, Technische Universität München, Habil.-Schr. (2012)
84. Thümmel, T., Ginzinger, L.: Measurements and simulations of a crank and rocker mechanism including friction, clearance and impacts. In: Proceedings of the IX. International Conference on the Theory of Machines and Mechanisms in Liberec/Czech Republic Aug. 31–Sept. 2004, pp. 763–768 (2004). Technical University of Liberec, Department of Textile Machine Design
85. Thümmel, T., Roßner, M.: Introduction to modelling and parameter identification methodology of linkages by measurements and simulation. In: Proceedings of the 13th World Congress in Mechanism and Machine Science, Guanajuato, Mexico, 19–25 June, vol. IMD–123 (2011)
86. Thümmel, T., Rutzmoser, J., Ulbrich, H., Robner, M.: Friction modeling and parameter value estimation of mechanisms. In: The 2nd Joint International Conference on Multibody Systems Dynamics, May 29–June 1, 2012, Stuttgart, Germany, pp. 302–312 (2012). University of Stuttgart, Institute of Engineering and Computational Mechanics
87. Ting, K.L., Zhu, J., Watkins, D.: The effects of joint clearance on position and orientation deviation of linkages and manipulators. Mech. Mach. Theory **35**(3), 391–401 (2000)
88. Varedi, S.M., Daniali, H.M., Dardel, M.: Dynamic synthesis of a planar slider–crank mechanism with clearances. Nonlinear Dyn. **79**(2), 1587–1600 (2015). doi:10.1007/s11071-014-1762-x
89. Yan, S., Xiang, W., Zhang, L.: A comprehensive model for 3D revolute joints with clearances in mechanical systems. Nonlinear Dyn. **80**(1), 309–328 (2015). doi:10.1007/s11071-014-1870-7
90. Zabiri, H., Samyudia, Y.: A hybrid formulation and design of model predictive control for systems under saturation and backlash. J. Process Control **16**, 693–709 (2006)
91. Zhang, H., Brogliato, B., Liu, C.: Dynamics of planar rocking-blocks with Coulomb friction and unilateral constraints: comparisons between experimental and numerical data. Multibody Syst. Dyn. **32**(1), 1–25 (2014)